Structural robustness quantification through the characterization of disproportionate collapse compared to the initial local failure

Mohammad El Hajj Diab, Cédric Desprez, André Orcesi, Jeremy Bleyer

Version of Record: https://www.sciencedirect.com/science/article/pii/S0141029622000293
Manuscript_c2e9373940779652d4d7ed5ccc0e070c

Structural robustness quantification through the characterization of disproportionate collapse compared to the initial local failure

Mohammad EL HAJJ DIAB [1], Cédric DESPREZ [2], André ORCESI [3]*, and Jérémy BLEYER[4]

ABSTRACT: Modern design codes recommend ensuring an appropriate level of robustness to prevent disproportionate collapse under an exceptional event. This concept directly refers to the capacity of limiting progressive collapse after an unexpected initial local failure. Assessing a structure in terms of robustness results in a complex issue as it not only requires information on the structural response in a large non-linearity domain, but also as it introduces a high level of uncertainty due to the concept of exceptional initial action. This study proposes a strategy to assess structural robustness using collapse propagation and energy-based indicators. A case study on a demonstrative steel frame building is presented. The first step consists in the definition of the possible scenarios leading to the loss of one or several structural element(s), such as columns. For each scenario, the structural response, including collapse propagation and alternative equilibrium is investigated using a fast computational modelling coupling the yield design theory and a non-linear finite element analysis. Initial to final damage ratios of the structural system and needed energy for initial failure are computed to quantify the robustness of the structure through this scenario-based analysis. A Pareto front analysis of the scenarios is then conducted by solving bi-objective problems that aim to maximize the collapse propagation and minimize the required demand of the initial local failure scenarios. The scenario-based and Pareto front analyses are applied to compare different structural design configurations of a case study used for illustration purpose. Results

[1] MAST-EMGCU, Univ Gustave Eiffel, IFSTTAR, F-77447 Marne-la-Vallée, France (now at ETANDEX, France)
[2] MAST-EMGCU, Univ Gustave Eiffel, IFSTTAR, F-77447 Marne-la-Vallée, France
[3]* [a]MAST-EMGCU, Univ Gustave Eiffel, IFSTTAR, F-77447 Marne-la-Vallée, [b]Cerema, DTecITM/DTOA, 77447 Champs-sur-Marne, France; corresponding author : E-mail : andre.orcesi@cerema.fr
[4] Navier, Univ Gustave Eiffel, ENPC, CNRS, F-77447 Marne-la-Vallée, France

clearly show how the two levels of analysis give complementary results that allow (i) quantifying and comparing robustness performance of the structure and (ii) identifying critical scenarios.

Keywords: structural robustness, numerical analysis, exceptional events, progressive collapse, disproportionate collapse, local failure.

1. Introduction

Structural robustness assessment is a complex process where definitions and assumptions can vary inside engineering or research communities. A consensus exists though in the concept of structural robustness proposed in design standards (NF EN 1991-1-7 2007, GSA 2003, 2013, DoD 2005, 2009, 2016, DCLG 2013, ASCE 2016). It refers to the ability of a structure to withstand an accidental or exceptional action, without being damaged to an extent disproportionate to the original cause. Structural robustness is not intended to protect the structure of any kind of actions at whatever magnitude, but rather to prevent an initial local failure, resulting from an unexpected action, to spread and lead to a disproportionate damage propagation.

Structural design against accidental or exceptional actions does not imply the same level of characterization of loads or actions. Demonceau (2008) and Huvelle (2011) distinguish the concepts of accidental and exceptional events. The accidental actions refer to the fully identified actions that are taken into account in the structural design (types and amplitudes of action). Conversely, exceptional actions refer to some actions that may be unknown during design due to a knowledge gap, or whose intensity could go beyond the expected magnitude. Similar concepts of accidental and exceptional actions are also referring to identified and unidentified accidental actions (NF EN 1991-1-7 2007). COST Action TU0601 (2011)

mentions that structural robustness aims to provide a sufficient structural resistance to survive to a failure that can be the loss of one of the critical structural elements (*fib* 2012). It characterizes the insensitivity of a structure to a local failure without propagation, where the failure of components other than those directly affected is unacceptable.

While the engineering community has adopted several design approaches to improve the structural robustness (Adam et al. 2018), including the tying method, the alternative load path (ALP) method, the specific local resistance design method, and the risk-based assessment method, the scientific community has thoroughly investigated the concept of robustness from different perspectives that can be summarized in the two following groups: the quantification of structural robustness through indicators, and the modelling of progressive collapse with numerical or experimental tests that reach or go beyond ultimate limits. The connection between both groups is the development of structural robustness concepts, in agreement with design standards, to improve and assess the resistance of structures against exceptional actions and avoid the catastrophic collapses (Foley et al. 2007, Vrouwenvelder 2008, Starossek & Haberland 2010, Alashker et al. 2010, Arup 2011).

Some measures or robustness were proposed either in a deterministic way or through a probabilistic approach, where the inherent uncertainties of the model are taking into account (relating to the material properties, the applied loads or the geometrical data) (Starossek & Haberland 2011). Several proposed robustness metrics compare a structure between undamaged and damaged conditions to assess the residual capacity to maintain some initial function after a damage occurs (Khandelwal and El-Tawil, 2011). Besides, (Izzuddin et al. 2007; Jaspart et al. 2011; Botte et al. 2014) have focused on the alternative load path approach to investigate whether the failure of some components with large displacements can lead to an alternative functioning (Brett and Lu 2013, Huvelle et al. 2015) and eventually prevent the cascading failure of other elements in the structure.

Another key aspect is to analyze the damage propagation within the structure with respect to the initial local failure (Faber 2007, Bontempi et al. 2007, Agarwal & England 2008, Biondini et al. 2008, fib 2012) as the structure should enable the safe evacuation of its users or occupants after the damage occurrence (Ghosn et al. 2016). Gerasimidis (2014), Sideri et al. (2016, 2017) and Pantidis et al. (2018) have worked on the vulnerability assessment of damaged systems to progressive collapse, also investigating the agreement between analytical methods finite element modelling of the structure. De Biagi (2020) recently investigated how the internal energy is redistributed within framed structures after element removal, showing the interest of energy-based approaches for the evaluation of robustness. Besides, Droogné et al. (2018) proposed a structural calculation framework that includes the interaction between the directly affected beams subjected to large deformations and the remaining indirectly affected part of the structure, showing the interest of a two-level reliability analysis.

Moreover, structural robustness depends not only on the types and amplitudes of action, but also on the frequency or probability of exceedance (Haberland 2007, JCSS 2008, COST Action TU0601 2011). Some robustness measures were proposed based on probabilistic risk assessment with the view to model the cascading failure feature of progressive collapse, recognizing the randomness in material, geometrical and loading parameters in a risk-based approach (Faber et al. 2006, Baker et al. 2008, Kagho Gouadjio et al. 2015). Droogné et al. recently took advantage of decomposing the structure in two parts to further reduce the computational cost of risk-based analyses, also using efficient simulation procedures such as Latin Hypercube sampling. Besides, Praxedes et al. (2021) focused on the development of a risk-based robustness index that considers the full spectrum of risk evolution after initiation of a triggering event. As one major drawback of this proposed index was the relative computational cost, Praxedes and Yuan (2021) focused on developing an efficient computation method using a novel directional simulation technique. They also considered

robustness-oriented structural optimization of reinforced concrete frames against progressive collapse within a two-stage optimization formulation (Praxedes and Yuan 2022) by (i) maximizing the structural robustness while minimizing the total additional reinforcement beyond the conventional design (bi-objective problem in a first tactical stage) and (ii) considering the decision maker's risk attitude through the use of the cumulative prospect theory (to determine final design in a second strategic stage).

Dealing with the quantification of progressive collapse after initial failure requires specific structural modelling strategies to take into account complex phenomena such as nonlinear geometry and material behavior, along with large computational cost (especially to investigate a large number of scenarios) and numerical convergence issues (Kiakojouri et al., 2020). Considering these observations, the motivation is to address two main challenges: the undefined origin of the initial failure, and the evaluation of failure propagation with either an alternative equilibrium or a progressive collapse of the structure. A major ambition is then to provide a framework that (i) opens the set of potential local failures as initial starting point, (ii) follows failure propagation to characterize progressive collapse, and (iii) avoids considering an infinity of initial local failures.

To do so, this approach considers a description of the extent of failure propagation through an iterative coupling between the yield design approach and a non-linear analysis that was introduced by El Hajj Diab et al. (2021). Background and key aspects are presented in Section 2. The main novelty of this iterative coupling is to rely on the yield design method to identify critical collapse mechanisms in various scenarios in a very efficient manner. Indeed, the yield design approach is able to provide lower and upper bound estimates of the partially damaged structure at very low computational cost. Combined with a local nonlinear analysis of the directly affected part, collapse propagation due to load redistributions and geometrical effects can be considered for a large number of scenarios. Depending on the intensity of

internal load redistributions, the failure mechanism obtained from the kinematic yield design approach may therefore involve only the directly affected part or, in some cases, involve a larger region outside the directly affected part. Section 3 proposes a strategy for structural robustness assessment with (i) two complementary robustness indices obtained from a scenario-based analysis, among which the Failure Propagation Index (FPI) that identifies the structural capacity to prevent cascading failure of other elements and the Energy Index (EI) that characterizes within an energy-based approach the critical level of local failure leading to some unacceptable consequences, and (ii) a Pareto front analysis of the scenarios to further discriminate the critical scenarios. This strategy is illustrated in Section 4 with a steel framed building case study to highlight how the approach can investigate a large number of scenarios and identify the critical ones. Then, Section 5 is dedicated to a comparative analysis of design options that shows the benefits of the proposed approach in a design context. Several strengthening options are considered for the studied building and structural robustness levels are assessed according to the proposed approach. The developed concepts should help structural engineers associate a robustness performance level to several design options for comparison purpose. It should also help find the critical elements in a structure, and then make appropriate decisions to improve its ability to prevent progressive collapse.

2. Numerical modelling background for progressive collapse

In a context of high uncertainty about the initial local failure, the proposed strategy aims to study a large number of structural local failure scenarios to identify the critical scenarios that lead to a disproportionate collapse. El Hajj Diab et al. (2021) proposed an original structural modelling strategy based on an iterative coupling between the yield design approach and a non-linear analysis, to simulate progressive collapse in a simplified way, yet modeling efficiently failure propagation (Figure 1).

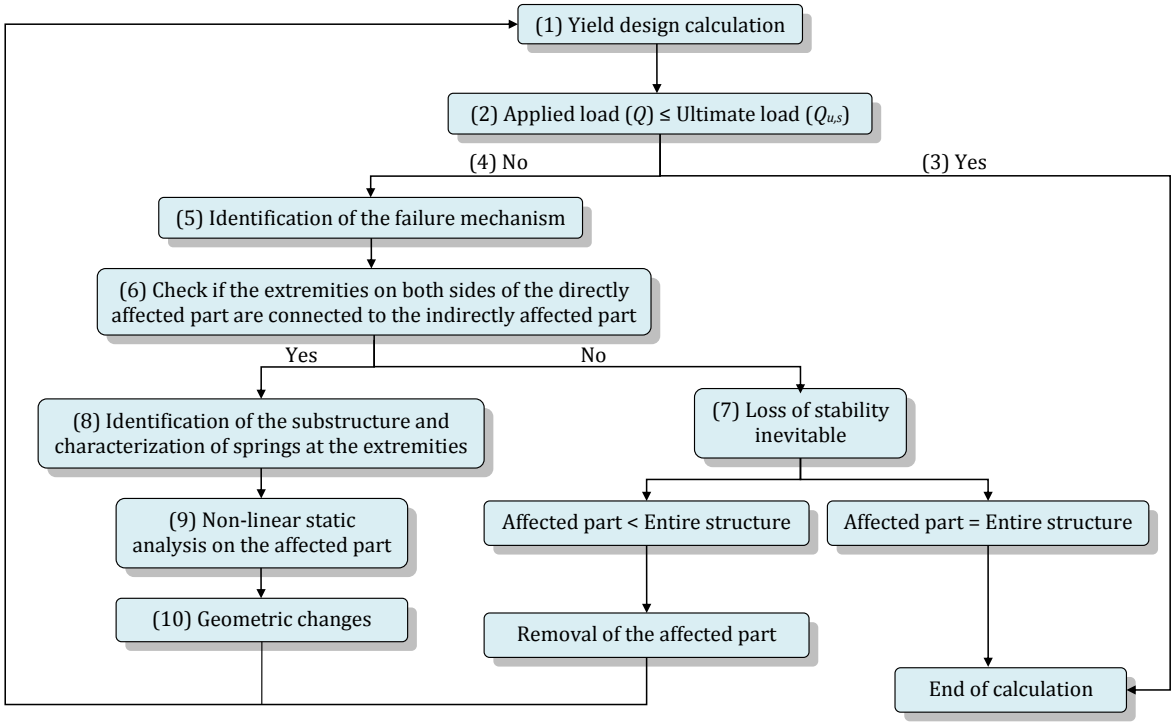

Figure 1. Proposed structural modelling strategy for progressive collapse analysis (El Hajj Diab et al. 2021).

Considering a structure after the occurrence of an initial failure (see the example in Figure 2), the yield design computation allows to approximate and surround the ultimate load Q_u. More precisely, the remaining structure after the removal of one or several column(s) is analyzed using the yield design method. Irrespective of the exact actions which led to the loss of some column(s), the external load pattern applied to the remaining structure is the same as the initial one (including a combination of dead loads and live loads), except that an additional dynamic amplification factor is applied to the directly affected area located just above the lost column(s). According to this prescribed load pattern, two different finite-element implementations (Bleyer & de Buhan, 2013) provide a lower bound estimate, the static ultimate load $Q_{u,s}$, and an upper bound estimate, the kinematic ultimate load $Q_{u,k} \geq Q_u$, respectively. The applied load Q (including the dynamic amplification factor due to the initial loss of element) is then compared with the lower limit $Q_{u,s}$. If $Q < Q_{u,s}$, the current structural configuration is assumed to stand the applied load without any damage. If $Q \geq Q_{u,s}$, the

structure is unable to resist and fails under the mechanism identified by the upper bound kinematic analysis.

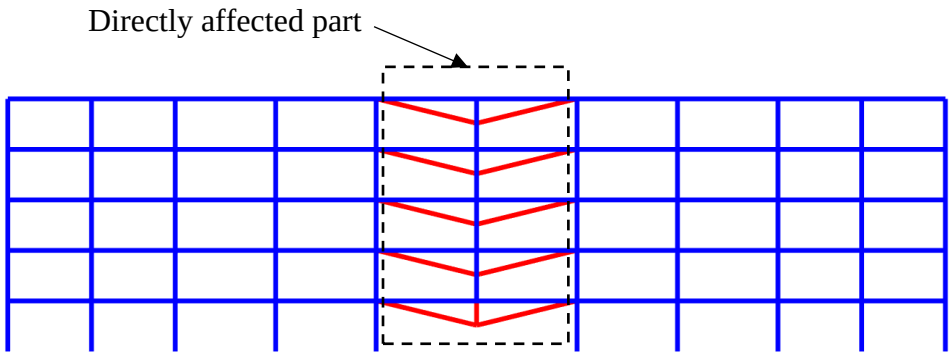

Figure 2. Example of scenario corresponding to the notional loss of a column in a frame building.

This mechanism identifies the directly affected part, and the critical points of the structure, where the structural element cannot resist the applied forces. It also enables to estimate whether there is a loss of stability of the directly affected part, or the possibility to develop an alternative functioning. In the former case, there is no interest to simulate the geometrical displacements of the affected part after the failure. In the latter case, the geometrical displacements might lead to a change in the redistribution of the forces in the elements, and the structure might be able to function in a different manner. Furthermore, this alternative functioning can increase the structural capacity to withstand the applied load. Therefore, there is an interest to simulate the geometrical changes in this case, and to study the evolution of the structural capacity with the geometrical displacements to investigate the ability of the structure to resist the applied load (El Hajj Diab 2019). In this respect, as the yield design approach is unable to simulate the geometrical non-linearities and identify the capacity of the structure to find an alternative equilibrium (i.e. arch or catenary actions) under large displacements, a non-linear finite element analysis is used to study the structural response of the part concerned by the initial failure mechanism. The development of an alternative functioning is then analyzed in the directly affected part, taking into account the geometrical

and the material non-linearities. Critical buckling loads are also verified according to Euler load formulation, in addition to strength limits based on the cross-section material properties (El Hajj Diab 2021). The successive iterations of the yield design approach with the deformed geometrical configuration allow to check the ability of the structure to develop a second line of defense that can lead to an alternative equilibrium.

The full description of this coupling strategy was presented in (El Hajj Diab et al. 2021) and applied to simulate the failure propagation under event-independent scenarios of loss of one or several column(s) in a steel frame case study. The structural responses under the applied scenarios were sorted into four categories. C1 category is without consequence as the local failure does not lead to any damage mechanism ; C2 category is without collapse of the directly affected part as a damage mechanism is initiated according to the yield design theory but the structure succeeds to find an alternative equilibrium ; C3 category concerns collapse of the directly affected part as the structure does not succeed to find a second line of defense. The damage mechanism leads to the failure of the concerned elements and to a partial collapse of the structure without further propagation beyond the first mechanism ; C4 category corresponds to a progressive collapse as the indirectly affected part of the structure cannot support the redistribution of loads in the new structural configuration and the collapse propagates out of the directly affected part. The coupling modelling strategy and scenarios sorting constitute the backbone of the approach presented in Section 3 and illustrated in Sections 4 and 5 with a case study.

3. Proposed strategy for robustness assessment

In order to quantify the structural robustness, two complementary levels of analyses are proposed. At a scenario-based level, two main performance aspects are quantified: the extent to which collapse propagates and the allowable capacity of the structure to face exceptional

events. The two corresponding indicators, based on the investigation of significant local failure scenarios allow a global assessment of the structure to mitigate progressive collapse. A Pareto front level analysis is then conducted to further discriminate critical scenarios. This second level of analysis holds on the research of three bi-objectives sets of scenarios (Pareto fronts) that simultaneously minimize the initial failure potential and maximize the final collapse extent.

3.1. Robustness index based on failure propagation

The first index is the Failure Propagation Index (FPI), which aims to quantify the structural capacity to prevent the propagation of a local failure. The first step is to identify the degree of failure propagation (DFP_i) for each applied scenario i (Figure 3), which is obtained by dividing a metric $\mathcal{M}(.)$ of the collapsed part after propagation of failure (CP_i) by the metric of the initially damaged part (IDP_i), as described in Equation 1:

$$\begin{cases} DFP_i = \dfrac{\mathcal{M}(CP_i)}{\mathcal{M}(IDP_i)} & if\ \mathcal{M}(IDP_i) \neq 0 \\ DFP_i = 0 & if\ \mathcal{M}(IDP_i) = 0 \end{cases} \quad (1)$$

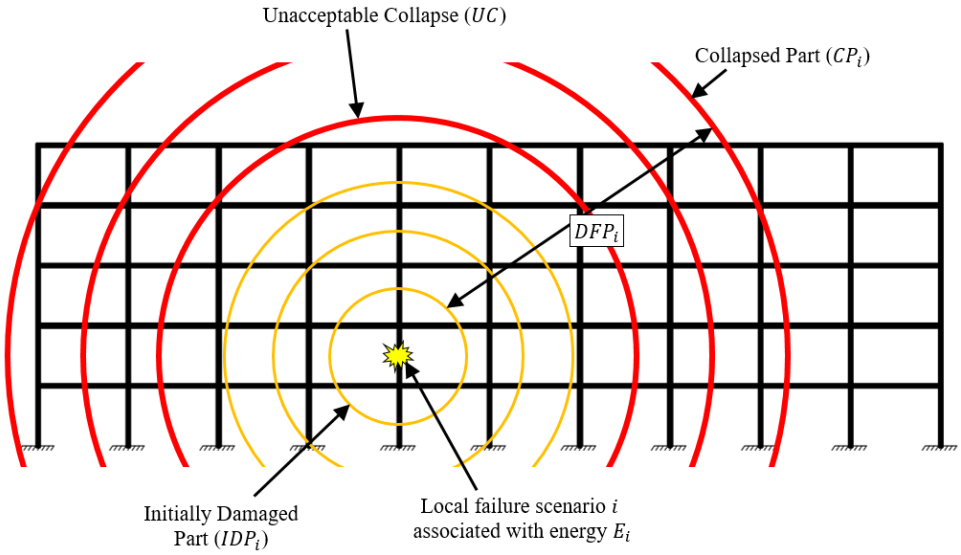

Figure 3. Characterization of the progressive collapse for scenario i.

Limiting the discussion to the case of a column loss scenario for a framed structure, the metric of the initially damaged part $\mathcal{M}(IDP_i)$ and the final collapsed part $\mathcal{M}(CP_i)$ can be practically quantified as the total length of affected beam (2D structure) or affected area of slab (3D structure). Such a metric aims at quantifying the damage propagation and enables to characterize, in a simple way, a disproportionate collapse threshold. Using Figure 2 as an example, the metric of the initially damaged part is the sum of beam lengths that are subject to a plastic mechanism in the directly affected part (El-Hajj-Diab et al. 2021). If $Q < Q_{u,s}$ (step 3 in Figure 1), there is no damage mechanism and $M(IDP_i) = 0$. If $Q \geq Q_{u,s}$ (step 4 in Figure 1), $M(IDP_i)$ corresponds to the cumulative length of beams concerned by the mechanism at the first iteration of the yield design computation. Besides, $\mathcal{M}(CP_i)$ corresponds to the cumulative length of collapsed beams in the last iteration of yield design (after coupling with non linear analysis). It can be either positive if some collapse occurs or equal to zero when an alternative equilibrium is reached without any collapse (for example, in Figure 2 if a catenary action can efficiently form in the beams).

Hence, the Degree of Failure Propagation (DFP_i) described in Equation 2 enables to quantify the propagation of a local failure, and the Failure Propagation Index (FPI), corresponds to the maximum degree of failure propagation among the N applied scenarios, as follows:

$$FPI = max\,\{DFP_i\,,\ \ i = 1, \dots, N\} \tag{2}$$

This index represents the worst case of failure propagation that may occur in the structure for the set of considered local failure scenarios, which gives an indication on how much the structure is prone to progressive collapse. The local failure scenarios with the largest propagation extent can be identified, as well as the way failure propagates, which identifies the critical elements of the structure that could be strengthened.

Further, the applied scenarios can be characterized as either acceptable or unacceptable according to Equation 3 where UC is a threshold for unacceptable collapse and CS is the corresponding set of critical scenarios.

$$CS = \{i \in [1, N] \; such \; that \; \mathcal{M}(CP_i) \geq UC\} \quad (3)$$

If no threshold is defined, UC can be assumed as the first $\mathcal{M}(CP_i)$ value that is greater than $\mathcal{M}(IDP_i)$, which means an initiation of progressive collapse.

3.2. Energy-based robustness index

In order to quantify the maximum capacity of structure to face exceptional events, a second index is proposed based on an energy approach that quantifies the sensitivity of the structure to the magnitude of the local initial failure scenario. Robustness assessment should consider not only the structural elements concerned by a local failure, but also the associated resistance capacity of these elements to withstand the action before failure. As the failure of a structural element occurs under an unknown action, the concept of reference load is introduced as a tool to rank scenarios of initial failure. It is proposed to use the associated energy required to cause the initial local failure of each scenario as an indicator to characterize the local failure scenario itself. In order to calculate the corresponding energy, the following points have to be specified: (i) type of loading (uniform, concentrated,…), (ii) other existing loads on the structural element, (iii) location of loading, (iv) affected elements (beams, columns…), (v) type of initial damage (total loss, cracking, corrosion,…), and (vi) boundary conditions of affected elements.

In the proposed approach, the required energy to cause the loss of an element is equal to the external work done by the reference load to reach the ultimate strain of the material. For example, the required energy to cause the failure of an element is expressed in terms of the

action load on the structural element and the element deformation, as described below (Izzuddin et al. 2008) :

$$E = \int \underline{Q}\, d\underline{u} \tag{4}$$

where E is the failure energy of the structural element according to the applied action, $\underline{Q}$ is the action load, and $\underline{u}$ is the displacement vector of the structural element.

A non-linear static analysis is performed to calculate the energy of the local failure scenario. The energy can be calculated according to different types of reference loads, as shown in Figure 4. Distributed loads (A_1, A_3, and A_4) can represent pressure effects, such as explosion and concentrated load (A_2) can represent an impact such as a vehicle collision.

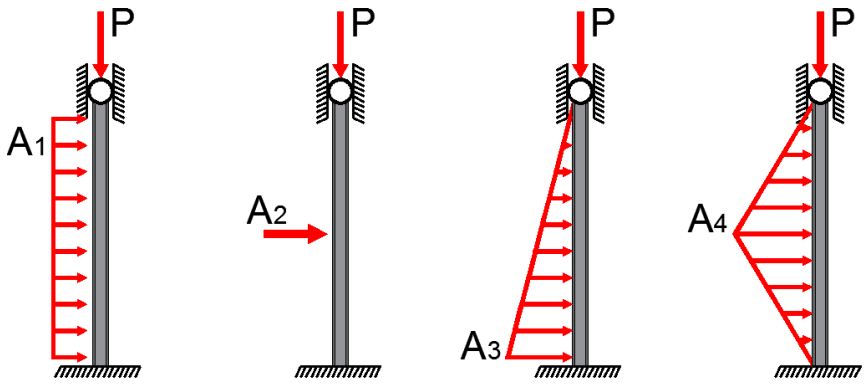

Figure 4. Applied loads to characterize the loss of a column.

As for the collapse propagation index, the threshold of unacceptable collapse allows identifying acceptable or unacceptable scenarios (Equation 3). The Energy Index $EI(UC)$ is then equal to the minimum energy value of the critical scenarios belonging to CS:

$$EI(UC) = min\{E_j, j \in CS\} \tag{5}$$

where E_j is the energy required to cause the j^{th} local failure scenario belonging to CS.

This index identifies the minimum level of energy needed to trigger a local failure scenario that could lead to an unacceptable collapse, based on the threshold UC defined beforehand. This aspect is essential since the scenarios leading to the greatest level of propagation do not

necessarily correspond to the scenario most likely to occur. Such an index can help reveal a potential lack of resistance in some critical elements (weak points of a structure to be strengthened), for which the failure under events that are relatively not significant in magnitude leads to an unacceptable propagation.

The previous indicators measure two different aspects of structural robustness, where FPI (based on DFP_i) focuses on the largest degree of failure propagation and $EI(UC)$ (based on E_i) focuses on the identification of the weakest point of the structure that leads to an unacceptable collapse. However, the set of scenarios can be discriminated by simultaneously looking for the maximal failure propagation potential and the minimal needed energy associated with the initial failure, since robustness can be understood as a combined research of minimal causes with maximal consequences. The research of Pareto fronts in the following is a strategy for such an identification.

3.3. Critical scenarios identification using Pareto fronts

Some methodology relying on the concepts of multi-objective optimization is proposed herein to find scenarios with minimal initial magnitude (based on energy or part of the structure initially affected) and maximal extent (based on failure propagation, or part of the structure that failed at the end). Indeed, looking for the critical scenarios aims to find scenarios that simultaneously present a high propagation level and a low capacity against the initial failure. To analyze the identification of critical scenarios among the wide interpretations of the propagation and disproportionate collapse notions, the proposed method considers three complementary bi-objective optimization problems.

First, scenarios sorting is done according to Equation 6 by (i) maximizing DFP_i, which refers to the largest collapse propagation ratio and (ii) minimizing E_i, which refers to the scenarios

with lowest magnitude of initial local failure. In this case, minimizing E_i is not associated to any threshold UC fixed beforehand.

$$\begin{cases} Find\ i = 1, \dots, N \\ max\{DFP_i\} \\ min\ \{E_i\} \end{cases} \quad (6)$$

Second, scenario sorting is done according to Equation 7 by (i) maximizing DFP_i and (ii) minimizing $\mathcal{M}(IDP_i)$, which refers to the scenarios with the lowest amplitude of initial local failure.

$$\begin{cases} Find\ i = 1, \dots, N \\ max\{DFP_i\} \\ min\ \{\mathcal{M}(IDP_i)\} \end{cases} \quad (7)$$

Third, scenarios sorting is done according to Equation 8 by (i) maximizing $\mathcal{M}(CP_i)$, which refers to the largest failure propagation (independently of the initial damaged part) and (ii) minimizing $\mathcal{M}(IDP_i)$.

$$\begin{cases} Find\ i = 1, \dots, N \\ max\{\mathcal{M}(CP_i)\} \\ min\ \{\mathcal{M}(IDP_i)\} \end{cases} \quad (8)$$

The three bi-objective problems are solved with the fast non-dominated sorting process proposed by Deb et al. (2002) according to Equations 9 and 10. If one denotes X the set of feasible decision vectors of the following optimization problem:

$$\begin{cases} Min\left(f_1(\underline{x}), f_2(\underline{x}), \dots f_k(\underline{x})\right) \\ such\ that\ \underline{x} \in X \end{cases} \quad (9)$$

it does not typically exist a feasible solution that simultaneously minimizes all objective functions and one looks for non-dominated solutions. A feasible solution $\underline{x}^1 \in X$ is said to dominate another solution $\underline{x}^2 \in X$, if

$$\begin{cases} f_i(\underline{x}^1) \leq f_i(\underline{x}^2) \text{ for all indices } i \in \{1,2,\dots,k\} \\ f_j(\underline{x}^1) < f_j(\underline{x}^2) \text{ for at least one index } j \in \{1,2,\dots,k\} \end{cases} \quad (10)$$

For each bi-objective problem p ($p = 1,2,3$), the non-dominated front, known as Pareto front, corresponds to the associated critical set of scenarios (Sp), where maximizing a function is considered by minimizing its negative. It is highlighted that the three proposed bi-objective problems do not necessarily lead to the same set of scenarios, as it is widely dependent on the objective functions under consideration. The choice of combining three complementary problem aims to cover three main interpretations about failure propagation after initial local failure. The total set of critical scenarios is obtained by merging the three sets S1, S2 and S3 where some scenarios can be present in one or several set(s). The critical scenarios belonging to the Pareto front scenarios (S1, S2 and S3) and also verifying $\mathcal{M}(CP_i) \geq UC$ (Figure 10) are then characterized as unacceptable scenarios. Sections 4 and 5 illustrate with a case study how structural robustness can be quantified, using the proposed indicators presented in Sections 3.1, 3.2 and 3.3.

4. Structural robustness assessment of a steel-framed building structure

This section investigates the robustness assessment of a typical steel-frame building subject to various columns losses. As the proposed method allows considering the initial failure sensitivity through an energy-based characterization, the influence of this input is formerly investigated. Then the multi-scenario analysis is performed to identify the critical scenarios in accordance with the proposed strategy.

4.1. Numerical mockup

The considered structure is a 2D typical five-storey steel-framed building with ten bays. The geometric layout of the structure is presented in Figure 5. The constitutive structural elements are IPE360 and HE500B cross-section profiles for beam and column respectively. Steel grade is S355, where the Young modulus (E) and yield strength (f_y) equals 210 GPa and 355 MPa, respectively.

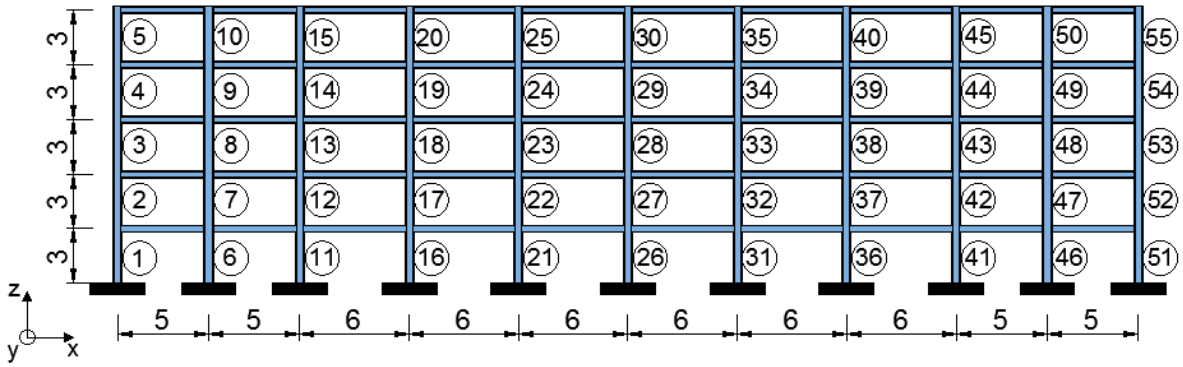

Figure 5. Layout of steel-frame building (dimensions in meter).

The beam/column and column/footing connexions are considered as rigid joints. The bay dimensions are 5 m or 6 m wide (*x* direction) and 4 m high (*z* direction). The floors consist of 25 cm reinforced concrete slabs carried by the steel beams. Gravity loads are determined considering a 4 m space between two consecutive bay in depth (*y* direction). Structural steel and reinforced concrete density for dead loads (DL) are 7850 kg/m^3 and 25 kN/m^3 respectively. Considering an administration building, the live loads (LL) are equal to 3 kN/m^2 according to the Eurocodes NF EN 1991-1-1 (2003). The beams are then exposed to uniform loads, where $DL = 25.6$ kN/m and live loads LL= 12 kN/m.

As robustness assessment is dedicated to exceptional events, an accidental action combination is assumed for further investigation. $W_a = DL + 0.5\,LL = 31.6$ kN/m for beams (NF EN 1990, 2003). Such a combination is selected for illustrative purpose, as there exists other combinations (Fu 2009), in particular when following GSA (2013) or DoD (2016) indications.

The vertical acceleration induced by instantaneous loss of columns is modeled through a dynamic equivalent amplification factor (DAF) set to 1.5 (Marchand and Alfawakhiri, 2005). This load amplification only concerns the directly affected part, which contains the beams and columns located just above lost column(s). Let us note that some studies can be considered for a more realistic choice of the DAF, taking into account the dissipation capacity of the structure (Ventura et al. 2018, De Biagi et al. 2020).

The finite element part of the progressive collapse analysis is performed using FEDEASLab software (Filippou & Constantinides 2004), a MATLAB toolbox. A multilayer beam element strategy is used to (i) take into account the material and geometrical non-linearities (Spacone et al. 1996) with a corotational formulation (Le et al. 2011, Le 2013, 2014) (ii) provide local information at the section level, and (iii) lower computational cost comparatively to a local approach regarding the need for multi-scenario analysis. To be consistent with the yield design calculation, the constitutive model for steel is assumed as a bilinear elastic, perfectly plastic relationship. Detailed information about the numerical tools and mockup are presented in (El Hajj Diab et al. 2021).

4.2. Characterization of local initial failure scenarios

The first step in the assessment procedure is to identify the initial local failure scenarios. In this case study, the total loss of one, two, three or four adjacent column(s) of the same level are considered. Table 1 shows the 190 resulting scenarios.

1	1	**33**	33	**65**	10 - 15	**97**	42 - 47	**129**	24-29-34	**161**	11-16-21-26
2	2	**34**	34	**66**	11-16	**98**	43-48	**130**	25-30-35	**162**	12-17-22-27
3	3	**35**	35	**67**	12-17	**99**	44-49	**131**	26-31-36	**163**	13-18-23-28
4	4	**36**	36	**68**	13-18	**100**	45-50	**132**	27-32-37	**164**	14-19-24-29
5	5	**37**	37	**69**	14-19	**101**	46-51	**133**	28-33-38	**165**	15-20-25-30
6	6	**38**	38	**70**	15-20	**102**	47-52	**134**	29-34-39	**166**	16-21-26-31

7	7	**39**	39	**71**	16-21	**103**	48-53	**135**	30-35-40	**167**	17-22-27-32
8	8	**40**	40	**72**	17-22	**104**	49-54	**136**	31-36-41	**168**	18-23-28-33
9	9	**41**	41	**73**	18-23	**105**	50-55	**137**	32-37-42	**169**	19-24-29-34
10	10	**42**	42	**74**	19-24	**106**	1-6-11	**138**	33-38-43	**170**	20-25-30-35
11	11	**43**	43	**75**	20-25	**107**	2-7-12	**139**	34-39-44	**171**	21-26-31-36
12	12	**44**	44	**76**	21-26	**108**	3-8-13	**140**	35-40-45	**172**	22-27-32-37
13	13	**45**	45	**77**	22-27	**109**	4-9-14	**141**	36-41-46	**173**	23-28-33-38
14	14	**46**	46	**78**	23-28	**110**	5-10-15	**142**	37-42-47	**174**	24-29-34-39
15	15	**47**	47	**79**	24-29	**111**	6-11-16	**143**	38-43-48	**175**	25-30-35-40
16	16	**48**	48	**80**	25-30	**112**	7-12-17	**144**	39-44-49	**176**	26-31-36-41
17	17	**49**	49	**81**	26-31	**113**	8-13-18	**145**	40-45-50	**177**	27-32-37-42
18	18	**50**	50	**82**	27-32	**114**	9-14-19	**146**	41-46-51	**178**	28-33-38-43
19	19	**51**	51	**83**	28-33	**115**	10-15-20	**147**	42-47-52	**179**	29-34-39-44
20	20	**52**	52	**84**	29-34	**116**	11-16-21	**148**	43-48-53	**180**	30-35-40-45
21	21	**53**	53	**85**	30-35	**117**	12-17-22	**149**	44-49-54	**181**	31-36-41-46
22	22	**54**	54	**86**	31-36	**118**	13-18-23	**150**	45-50-55	**182**	32-37-42-47
23	23	**55**	55	**87**	32-37	**119**	14-19-24	**151**	1-6-11-16	**183**	33-38-43-48
24	24	**56**	1-6	**88**	33-38	**120**	15-20-25	**152**	2-7-12-17	**184**	34-39-44-49
25	25	**57**	2-7	**89**	34-39	**121**	16-21-26	**153**	3-8-13-18	**185**	35-40-45-50
26	26	**58**	3-8	**90**	35-40	**122**	17-22-27	**154**	4-9-14-19	**186**	36-41-46-51
27	27	**59**	4-9	**91**	36-41	**123**	18-23-28	**155**	5-10-15-20	**187**	37-42-47-52
28	28	**60**	5-10	**92**	37-42	**124**	19-24-29	**156**	6-11-16-21	**188**	38-43-48-53
29	29	**61**	6-11	**93**	38-43	**125**	20-25-30	**157**	7-12-17-22	**189**	39-44-49-54
30	30	**62**	7-12	**94**	39-44	**126**	21-26-31	**158**	8-13-18-23	**190**	40-45-50-55
31	31	**63**	8-13	**95**	40-45	**127**	22-27-32	**159**	9-14-19-24		
32	32	**64**	9-14	**96**	41-46	**128**	23-28-33	**160**	10-15-20-25		

Table 1. Local failure scenarios for the steel-framed building structure (scenarios in bold and corresponding removed column number(s), see Figure 5).

The second step is to characterize the initial failure energy of columns according to Equation 4, the initial failure load path and the vertical acting load. The failure energy E is computed in accordance with boundary conditions of Figure 4, considering accidental load path for axial force. The displacement $\underline{u}$ is assumed to correspond to the element failure when the material strain reaches its ultimate value estimated by $\varepsilon_u = 20\varepsilon_y = 34‰$ (Brozzetti 1996). As an example, Table 2 shows energies and horizontal deflection values for the loss of column #26 under A1 to A4 loadings. In this initial configuration, axial load $P = 948$ kN.

Loading type	A_1	A_2	A_3	A_4

Energy (kJ)	80.6	97.9	66.2	91.3
Deflection δ_c (mm)	21.8	24.4	17.5	22.6

Table 2. Failure energy and horizontal deflection of column # 26 under the reference load types A1, A2, A3 and A4.

Testing the different loading types gives information about element sensitivity against actions, however it does not influence the ranking between the tested scenarios (El Hajj Diab 2019). The uniformly distributed load A_1 is then chosen in the following to characterize initial local failure energy of scenarios, the energy of a scenario with multiple losses being equal to the sum of the individual failure energies. This assumption is made, as the study does not focus on the description of a specific hazard, but deals with the use of energy as one of the assessment input. As the needed energy depends on the vertical load, the failure energy increases as *P* decreases. Table 3 shows for each column, the initial concentrated load *P* and the failure energy values.

Column #	Vertical load (*P*) (kN)	Energy (kJ)
1; 51	395.0	100.4
2; 52	316.0	102.1
3; 53	237.0	103.8
4; 54	158.0	105.4
5; 55	79.0	108.6
6; 46	790.0	84.2
7; 47	632.0	87.8
8; 48	474.0	98.8
9; 49	316.0	102.1
10; 50	158.0	105.4
11; 41	869.0	82.5
12; 42	695.2	86.1
13; 43	521.4	98.6
14; 44	347.6	102.0
15; 45	173.8	105.4
16; 21; 26; 31; 36	948.0	80.6
17; 22; 27; 32; 37	758.4	84.4
18; 23; 28; 33; 38	568.8	97.0
19; 24; 29; 34; 39	379.2	101.9
20; 25; 30; 35; 40	189.6	105.4

Table 3. Vertical load *P* and failure energy of each column #.

4.3. Identification of progressive collapse scenario

For each scenario, the progressive collapse computation is performed according to the coupling approach presented by El Hajj Diab et al. (2021). The structural response is then expressed according to the $\mathcal{M}(IDP_i)$ and $\mathcal{M}(CP_i)$ metrics that quantify the initial damage part (immediately after the initial loss of element) and final collapse part, respectively at the first and last iteration of yield design computation. Figure 6 shows the initial damaged part and final collapse measures for the 190 tested scenarios.

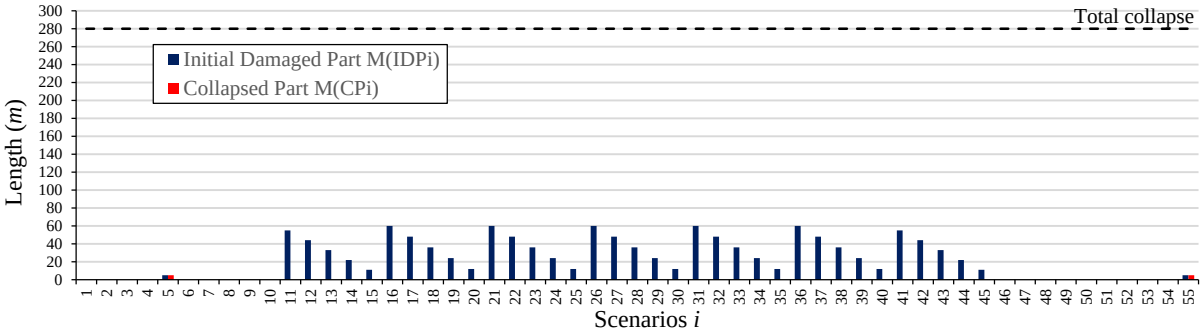

(a) Scenarios i with the loss of one column

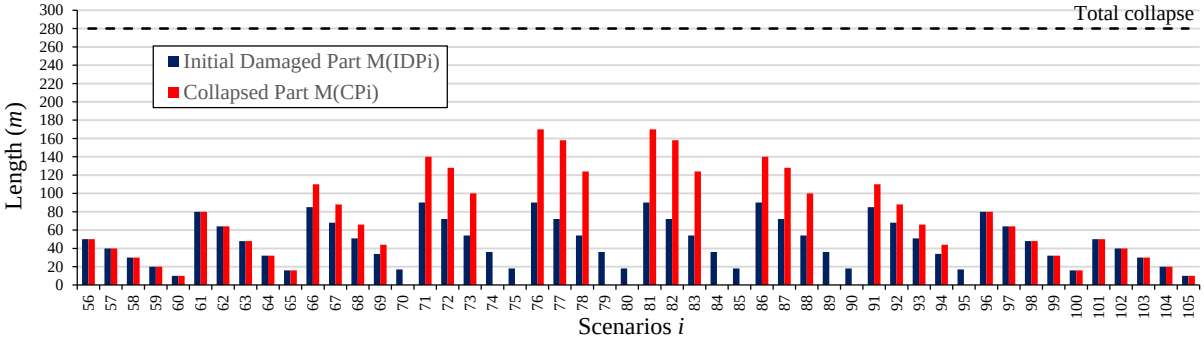

(b) Scenarios i with the loss of two columns

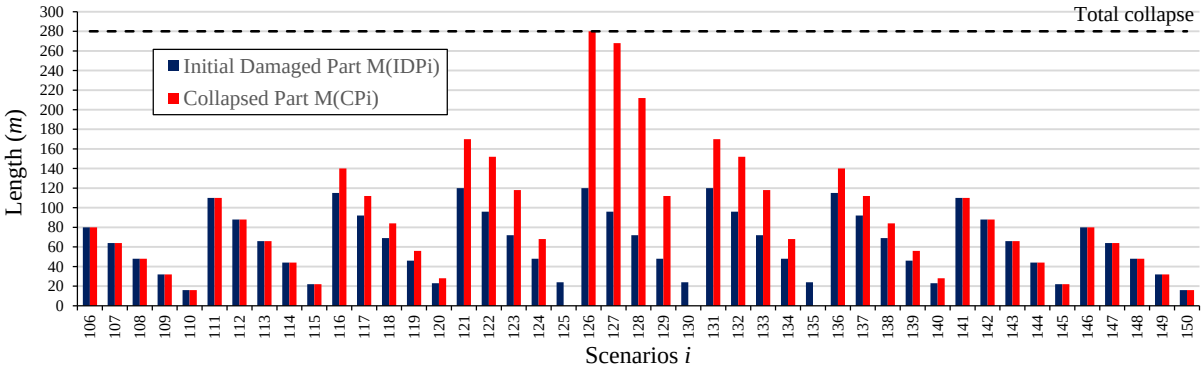

(c) Scenarios i with the loss of three columns

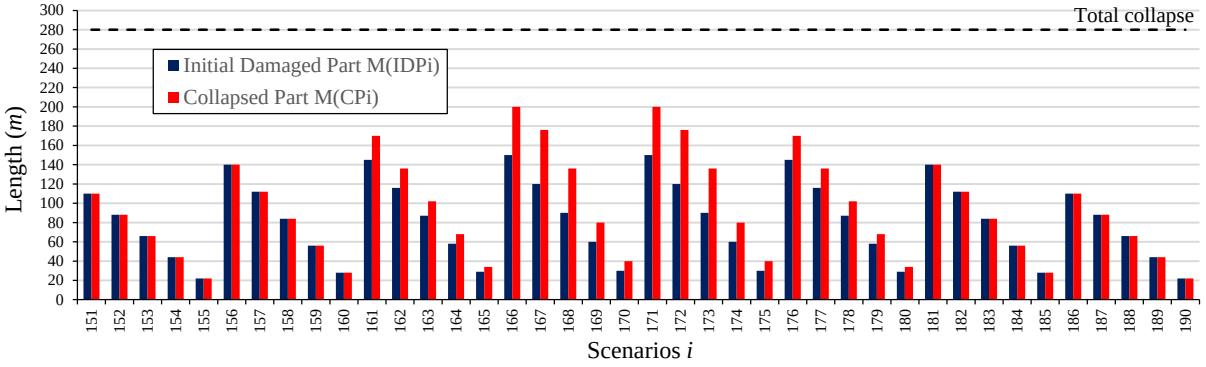

(d) Scenarios i with the loss of four columns

Figure 6. Measure of IDP_i and CP_i for each scenario i of local failure of Table 1.

Comparing the values of $\mathcal{M}(IDP_i)$ and $\mathcal{M}(CP_i)$, one observes the presence of scenarios that correspond to the four propagation categories identified previously : C1 (without consequences), C2 (with damage initiation, but without collapse of the directly affected part), C3 (with collapse of the directly affected part) and C4 (with collapse propagation out of the directly affected part). Table 4 shows the number of scenarios that corresponds to each category.

Categories	C1	C2	C3	C4
Loss of 1 column	18	35	2	0
Loss of 2 columns	0	10	20	20
Loss of 3 columns	0	3	20	22
Loss of 4 columns	0	0	20	20
Total	18	48	62	62

Table 4. Number of local failure scenarios within categories C1 to C4.

The structure can resist under most of the scenarios with the loss of one column, where it can perfectly resist without any consequences (C1) or it can resist by developing the tensile membrane action (C2). However, the loss of column # 5 or 55 makes the upper beam as a cantilever mechanism that leads to the collapse of the directly affected part. Therefore, these two scenarios fall in category C3.

The structure achieves to resist ten scenarios with the loss of two columns ($i = 70, 74, 75, 79, 80, 84, 85, 89, 90, 95$) by developing the tensile membrane action in beams (category C2).

Considering the loss of three columns, only the scenarios $i = 125, 130$ or 135 that affect the top floor lead to an alternative equilibrium of the structure, where the tensile membrane action in beams helps to avoid progressive collapse (category C2).

Apart from these scenarios, the loss of more than two columns always leads to some progressive collapse in the structure, where all scenarios fall in the categories C3 and C4. In particular, the total collapse of the structure occurs with the scenario $i = 126$ with the loss of columns # 21, 26 and 31 as it consists in removing three columns according to the symmetric axis of the structure, which leads to a symmetric collapse of both sides of the structure. However, it is interesting to note that the scenarios $i = 166$ and 171 do not lead to a total collapse, even if they both include columns 21, 26 and 31 as removing a fourth column creates a dissymmetric loading and capacity of the structure that partially collapses on its weakest side.

Table 5 illustrates the computation time related to the number of iterations both for yield design calculation ($n_{YD,i}$) and non-linear analysis ($n_{NL,i}$) realised to model the structural response of each scenario. Two types of scenarios are distinguished within category C3. In the first type (C3,1), the initially affected part has no possibility to develop an alternative equilibrium, so the non-linear analysis is not used, and two iterations of yield design calculation are realized, one for the initially affected part, and a second one to check if another failure mode develops in the rest of the structure. In the second type (C3,2), a non-linear analysis is performed to test the effect of the catenary action. The total computation time to study these 190 scenarios is 29.5 hours (1 processor 3.6GHz quadricore, 32 Go RAM).

Category		$n_{YD,i}$	$n_{NL,i}$	T_i
C1		1	0	14 s < T_i^{C1} < 15 s
C2		2	1	132 s < T_i^{C2} < 746 s
C3	C3,1	2	0	20 s < $T_i^{C3,1}$ < 29 s
	C3,2	3	1	118 s < $T_i^{C3,2}$ < 2156 s
C4		3	1	141 s < T_i^{C4} < 1894 s

Table 5. Number of iterations realised for each category of scenarios with the interval of computation time.

4.4. Calculation of robustness indices at the scenario-based level

The following step in the proposed methodology for robustness assessment aims to quantify the performance at a scenario-based level through a bi-indicator approach with the calculation of FPI and EI. In order to determine FPI, the degree of failure propagation (DFP_i) for each scenario i is calculated according to Equation 2. Table 6 presents the maximum degree of failure propagation regarding the number of removed columns. The highest value (2.9) corresponds to the scenario $i = 128$ with the loss of three columns. It is interesting to note that removing four columns, which corresponds herein to the largest initially affected part of the structure leads to a lower failure propagation. There are two reasons for this result. First, the more columns are removed in a scenario i, the larger is the initially affected part (IDP_i), which mathematically decreases the degree of failure extent. Second, as explained in the previous section, some scenarios based on the loss of three elements can lead to a larger propagation than when removing four due to the symmetry of the structure.

As the collapse propagation index is equal to the maximum degree of failure propagation among the applied scenarios (Equation 3), $FPI = 2.9$ in this example.

	Loss of 1 column	Loss of 2 columns	Loss of 3 columns	Loss of 4 columns
Max (DFP_i)	1	2.3	2.9	1.5

Table 6. Maximum value of degree of failure propagation according to the number of removed columns.

The Energy Index $EI(UC)$ is equal to the minimum energy value of the unacceptable scenarios. Figure 7 shows the local failure energy E_i and the measure $\mathcal{M}(CP_i)$ of the collapsed part for each applied scenario i. In this example, the threshold used to determine an unacceptable collapse in Equation 3 is fixed at 90 m, which arbitrary represents a third of the structure. Hence, $EI(UC = 90\text{ m}) = 161.2$ kJ. This index identifies the scenario with the lowest magnitude in energy E_i that leads to an unacceptable failure. In this example, it refers to the scenarios with the loss of two columns: $i = 71$, 76, 81 or 86 (see Table 1). In this set, scenarios 76 and 81 have the highest FPI.

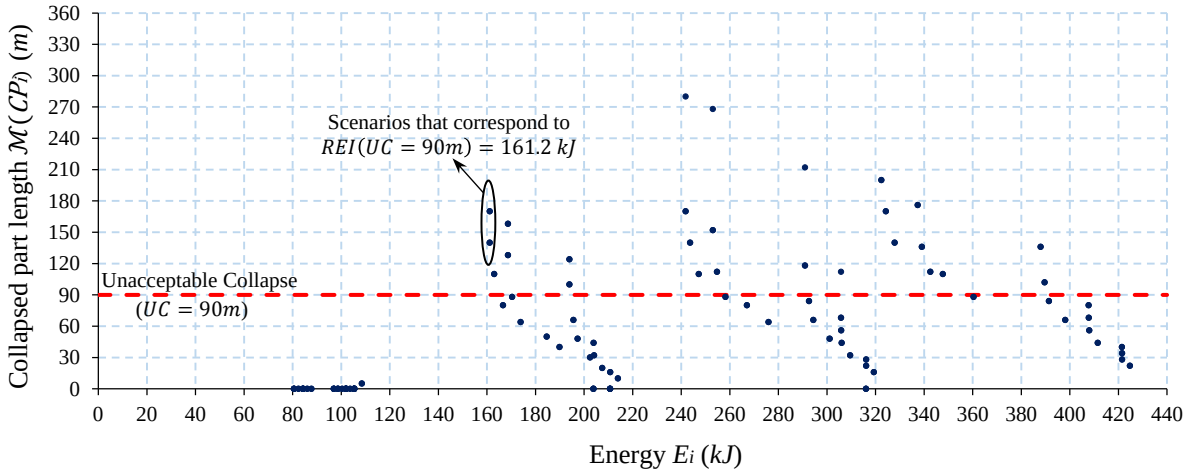

Figure 7. Local failure energy – collapsed part length diagram.

4.5. Robustness analysis at the Pareto front level

Failure propagation and energy needed for initial failure are two distinct aspects that can also be analyzed together at a Pareto front level according to the three bi-objectives problems presented in Equations 6, 7 and 8. Considering the first situation, Equation 6 is used to sort scenarios by maximizing DFP_i and minimizing E_i. The classification of tested scenarios are presented in Figure 8, where the diameter of the bubbles refers to the successive number of non-dominated fronts according to Equation 10 (largest diameter is for the Pareto front). Table 7 details the eleven non-dominated scenarios constitutive of the Pareto front S1.

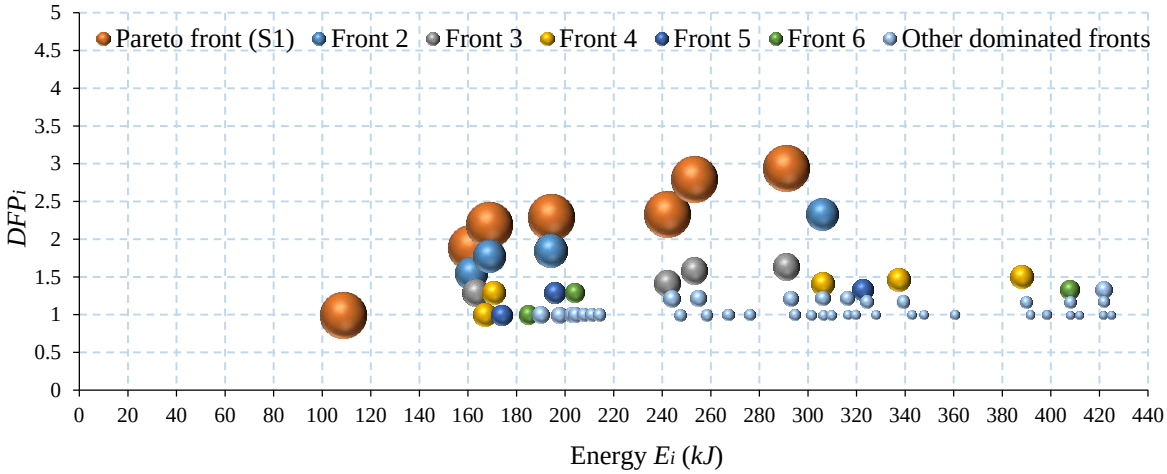

Figure 8. Identification of non-dominated scenarios when simultaneously minimizing E_i and maximizing DFP_i (Equation 6).

Scenario i	Column #	E_i (kJ)	DFP_i
5	5	108.6	1.0
55	55	108.6	1.0
76	21-26	161.2	1.9
81	26-31	161.2	1.9
77	22-27	168.7	2.2
82	27-32	168.7	2.2
78	23-28	194.0	2.3
83	28-33	194.0	2.3
126	21-26-31	241.9	2.3
127	22-27-32	253.1	2.8
128	23-28-33	291.0	2.9

Table 7. Non-dominated scenarios (Pareto front S1) related to Equation 6.

The structural robustness can also be studied by identifying the maximum failure propagation DFP_i with the minimal initial damaged part $\mathcal{M}(IDP_i)$, according to Equation 7. Table 8 shows the results of this bi-objective problem that leads to eight non-dominated scenarios (Pareto front S2).

Scenario i	Column #	$\mathcal{M}(IDP_i)$ (m)	DFP_i
5	5	5	1.0
55	55	5	1.0
120	15-20-25	23	1.2
140	35-40-45	23	1.2
170	20-25-30-35	30	1.3

175	25-30-35-40	30	1.3
129	24-29-34	48	2.3
128	23-28-33	72	2.9

Table 8. Non-dominated scenarios (Pareto front S2) related to Equation 9.

Finally, a third scope of analysis consists in identifying the scenarios that maximize the final collapsed part $\mathcal{M}(CP_i)$ and minimize initial damaged part $\mathcal{M}(IDP_i)$ according to Equation 8. Thirty non-dominated scenarios are identified (Pareto front S3) and presented in Table 9.

Scenario # i	Column #	$M(IDP_i)$ (m)	$M(CP_i)$ (m)
5	5	5	5
55	55	5	5
60	5-10	10	10
105	50-55	10	10
65	10-15	16	16
100	45-50	16	16
110	5-10-15	16	16
150	45-50-55	16	16
59	4-9	20	20
104	49-54	20	20
115	10-15-20	22	22
145	40-45-50	22	22
155	5-10-15-20	22	22
190	40-45-50-55	22	22
120	15-20-25	23	28
140	35-40-45	23	28
165	15-20-25-30	29	34
180	30-35-40-45	29	34
170	20-25-30-35	30	40
175	25-30-35-40	30	40
69	14-19	34	44
94	39-44	34	44
119	14-19-24	46	56
139	34-39-44	46	56
129	24-29-34	48	112
78	23-28	54	124
83	28-33	54	124
128	23-28-33	72	212
127	22-27-32	96	268
126	21-26-31	120	280

Table 9. Non-dominated scenarios (Pareto front S3) related to Equation 10.

To illustrate the fact that the non-dominated status of scenarios strongly depends on the choice of the bi-objective problem in Equations 6, 7 and 8, the solutions S1, S2 and S3 are represented in the diagrams $E_i - DFP_i$, $\mathcal{M}(IDP_i) - DFP_i$, and $\mathcal{M}(IDP_i) - \mathcal{M}(CP_i)$ in Figures 9a, b and c, respectively. First, the critical scenarios can be easily identified, finding

those with the lowest initial magnitude (E_i or $\mathcal{M}(IDP_i)$ in x axis) or those with the largest failure extent (DFP_i or $\mathcal{M}(CP_i)$ in y axis). Second, it illustrates how far some critical scenarios can be from the Pareto front obtained with some specific objective functions. Figure 9a shows that some solutions of S2 and S3 have a relatively low DFP_i index, compared to solutions S1. This result is explained, as minimizing $\mathcal{M}(IDP_i)$ does not necessarily correspond to the solutions with lowest energy level. Indeed, minimizing local failure energy leads to scenarios of column loss in the lower stories of the structure as the failure energy increases when the concentrated load on columns decreases (Table 3). Conversely, minimizing $\mathcal{M}(IDP_i)$ leads to scenarios of column loss in the upper stories of the structure where the directly affected part is smaller. Such consideration explains why the majority of S1 solutions in (Figures 9b and 9c) are on the right side of the x axis. Solutions S2 and S3 are more grouped in these two figures. Besides, in Figure 9b, the critical scenarios identified when maximizing DFP_i (Pareto front S2) are among the set of scenarios of solution S3 (Tables 8 and 9) when maximizing $\mathcal{M}(CP_i)$. Indeed, simultaneously minimizing $\mathcal{M}(IDP_i)$ and maximizing $\mathcal{M}(CP_i)$ is close to minimizing $\mathcal{M}(IDP_i)$ and maximizing DFP_i. However, the results of these problems are different due the fact that the DFP_i is a relative difference between the directly affected part and the one at the end of the failure propagation.

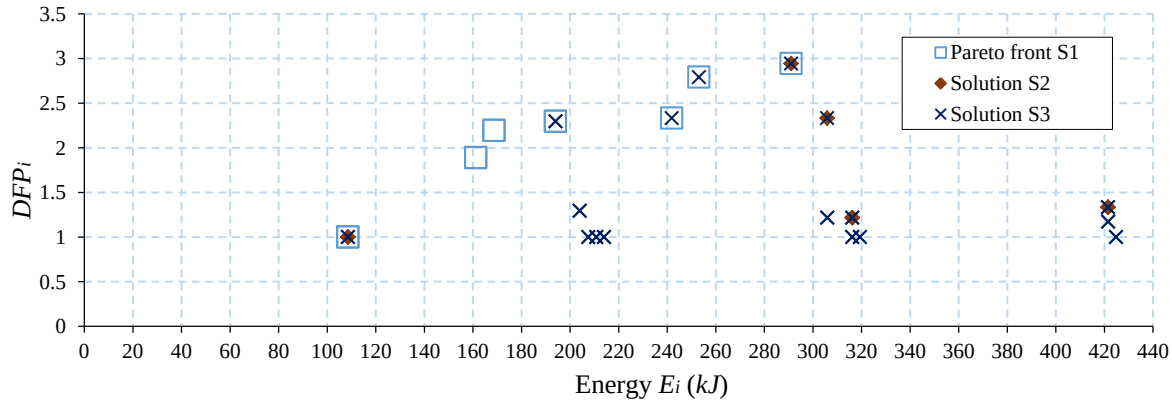

(a) E_i -DFP_i diagram

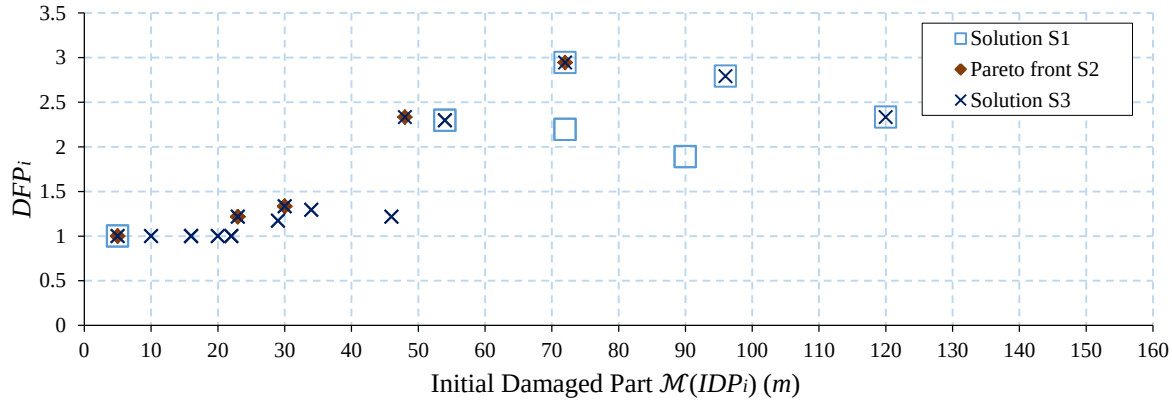

(b) $M(IDP_i)$-DFP_i diagram

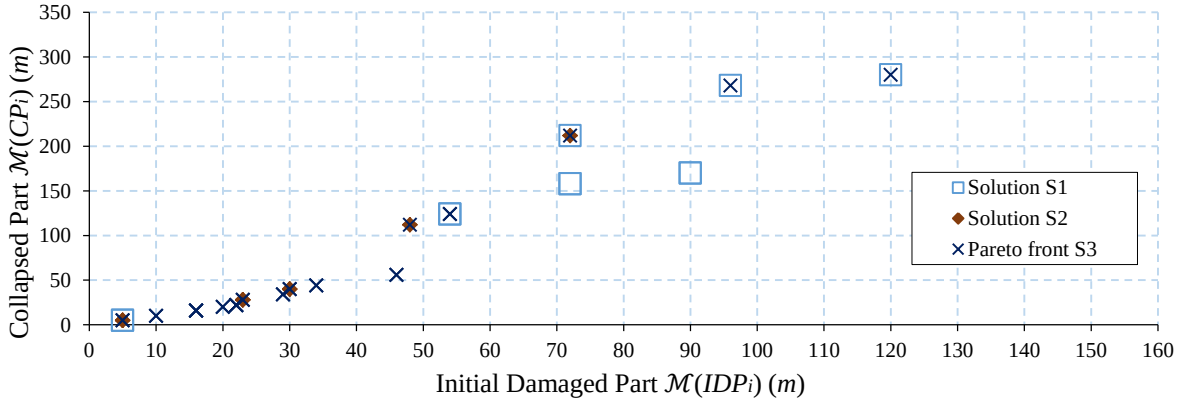

(c) $\mathcal{M}(IDP_i)$- $\mathcal{M}(CP_i)$ diagram

Figure 9. Pareto fronts S1, S2 and S3 in (a) E_i -DFP_i diagram, (b) $M(IDP_i)$-DFP_i diagram, and (c) $\mathcal{M}(IDP_i)$-$\mathcal{M}(CP_i)$ diagram.

The three Pareto fronts lead to identifying 34 distinct critical scenarios that simultaneously maximize damage propagation and minimize the magnitude of the local failure among the 190 scenarios of Table 1. However, these critical scenarios are not necessarily unacceptable if the final collapse part remains lower than the threshold associated to an unacceptable extent of progressive collapse. Further investigations are proposed thereafter to address this question.

The proposed notion of unacceptable scenario refers to the set of critical scenarios that belong to the Pareto fronts S1, S2, or S3 and that overpass a defined damage threshold. The first scenario-based level of analysis (without threshold) leads to 124 scenarios where $DFP_i \geq 1$, corresponding to C3 and C4 categories (Table 4). In this case, a particular set of critical scenarios are the common ones between the 34 Pareto front scenarios (S1, S2 and S3) and the

124 scenarios C3 and C4. This strictly leads to the 34 Pareto scenarios as shown in Figure 10 and Table 10. A second level of analysis (with threshold) corresponds to 48 of the 124 previous scenarios where $\mathcal{M}(CP_i) \geq 90$ m (assuming the same threshold than for $EI(UC)$). The unacceptable scenarios are then the common scenarios between the 34 Pareto front scenarios (S1, S2 and S3) and the 48 scenarios of this second set. Ten scenarios are identified (Figure 10, Table 10).

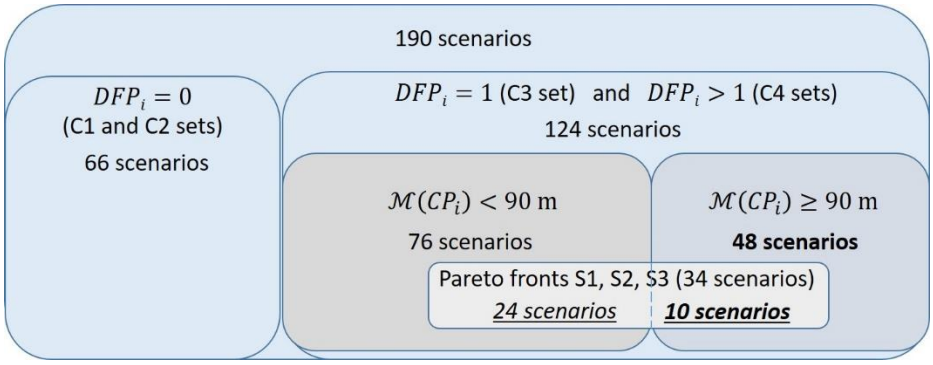

Figure 10. Discrimination of critical/unacceptable scenarios.

Scenarios of C3 and C4 categories ($DFP \geq 1$)

56	57	58	61	62	63	64	67	68	92	93	96	97	98	99	101
102	103	106	107	108	109	112	113	114	118	124	134	138	142	143	144
146	147	148	149	152	153	154	158	159	160	164	169	174	179	183	184
185	187	188	189	*5*	*55*	*59*	*60*	*65*	*69*	*94*	*100*	*104*	*105*	*110*	*115*
119	*120*	*139*	*140*	*145*	*150*	*155*	*165*	*170*	*175*	*180*	*190*	***76***	***77***	***78***	***81***
82	***83***	***126***	***127***	***128***	***129***	**66**	**71**	**72**	**73**	**86**	**87**	**88**	**91**	**111**	**116**
117	**121**	**122**	**123**	**131**	**132**	**133**	**136**	**137**	**141**	**151**	**156**	**157**	**161**	**162**	**163**
166	**167**	**168**	**171**	**172**	**173**	**176**	**177**	**178**	**181**	**182**	**186**				

Table 10. Identification of the 124 scenarios of C3 and C4 categories (DFP≥1) – (a) In bold : $\mathcal{M}(CP_i) \geq 90$ m (48 scenarios) – (b) In Italic underlined : Pareto fronts S1, S2 and S3 (34 scenarios) – grey background : common scenario between (a) and (b).

This second level of analysis allows sorting the scenarios as follows. Amongst the 190 tested scenarios, 124 (65 %) lead to failure propagation and partial or total collapse of the structure, 48 (25 %) lead to an unacceptable progressive collapse, including 10 non-dominated Pareto

scenarios (5 %) particularly critical, as they maximize progressive collapse and minimize local failure magnitude. This critical set contains the 3 scenarios ($i = 76, 81, 128$) previously identified with robustness indices FPI and EI.

5. Comparison of different structural configurations using robustness indices

Variations about the steel-framed building of Section 4 are used to illustrate how the proposed approach can help to compare different structural design configurations or strengthening. As the steps of the approach are already detailed in Section 4, only the main results and conclusions are presented thereafter (full results are available in El Hajj Diab, 2019).

5.1. Design configurations

Five configurations are considered: D0 (initial configuration), D1 (beams upgrade), D2 (columns upgrade), D3 (beams and columns upgrade), and D4 (braces upgrade with rigid connections). Table 11 details the five configurations and Figure 11 gives a view of D4 configuration where it is assumed that the column loss also leads to the loss of its connections with braces.

	D0	D1	D2	D3	D4
Beam	IPE360	IPE550	IPE360	IPE550	IPE360
Column	HE500B	HE500B	HE800B	HE800B	HE500B
Braces	No	No	No	No	Square Hollow Sections 150 x 150 x 6 mm – S235

Table 11. Identification of configurations D0, D1, D2, D3 and D4.

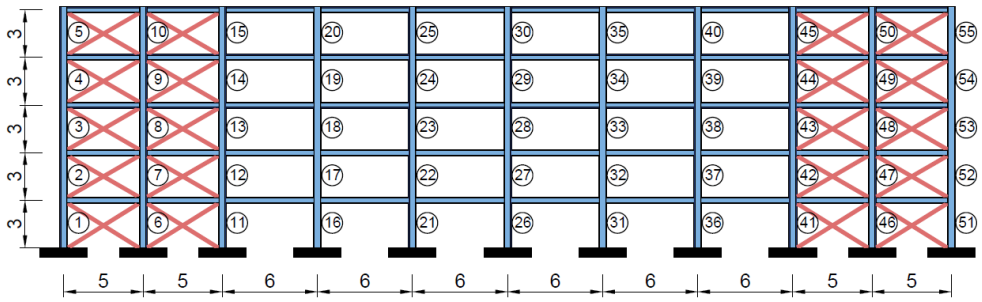

Figure 11. Layout of design configuration D4 (dimensions in meter).

5.2. Analysis of structural robustness

As for the initial structure D0, all the 190 initial local failure scenarios (Table 1) are investigated for D1 to D4. The structural response is determined each time using the coupling between yield theory and non-linear finite element analysis. E_i, $\mathcal{M}(IDP_i)$, $\mathcal{M}(CP_i)$, and $DFPi$ are computed for each scenario to determine CPI and $EI(UC = 90\text{ m})$ as well as the associated scenarios (Tables 12 and 13). Figure 12 shows that D0 and D3 are respectively the weakest and strongest configurations. Indeed, D0 gives the highest value of FPI (2.9) and lowest value of $EI(UC = 90\text{ m})$ (161.2 kJ) while D3 gives the lowest value of FPI (2.3) and highest value of $EI(UC = 90\text{ m})$ (386.8 kJ).

	D0	D1	D2	D3	D4
FPI	2.9	2.8	2.9	2.3	2.8
Scenario i	128	127	128	126	128

Table 12. *FPI* values and associated scenarios for D0 to D4 configurations.

	D0		D1		D2		D3		D4	
$EI(UC = 90\text{ m})$ (kJ)	161.2		241.7		257.9		386.8		161.2	
Scenario i	71, 86	76, 81	121, 131	126	71, 86	76, 81	121, 131	126	71, 86	76, 81
CP_i (m)	140	170	170	280	140	170	170	280	140	170

Table 13. $EI(UC = 90\ m)$ values and associated scenarios for D0 to D4 configurations.

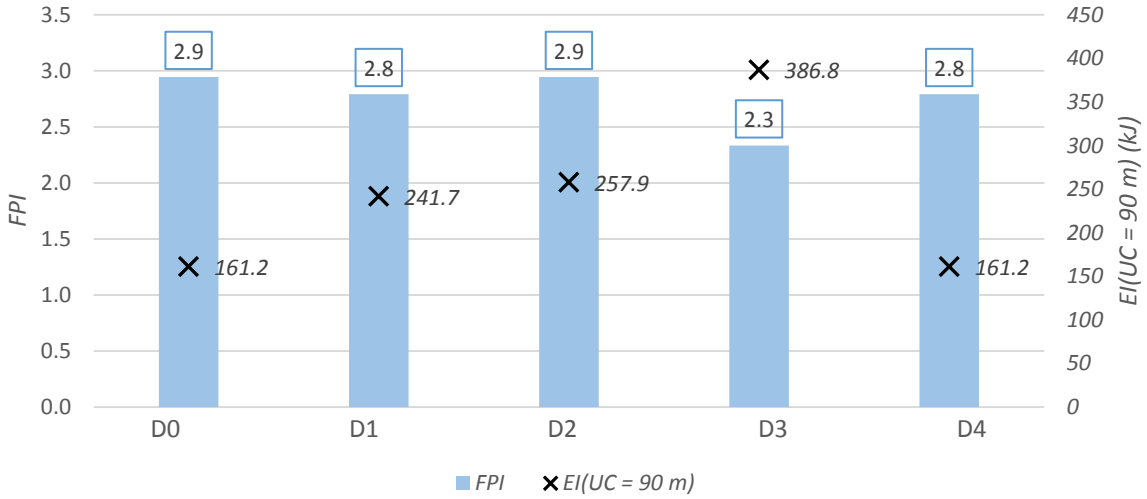

Figure 12. FPI (left axis) and $EI(UC = 90\ m)$ (right axis) indices for D0, D1, D2, D3 and D4 configurations.

$\mathcal{M}(IDP_i)$, $\mathcal{M}(CP_i)$, $DFPi$ are also used to directly identify the ratio of each collapse category C1 to C4 for the different configurations (Figure 13). Considering the C3 and C4 scenarios (partial or total collapse), it indicates that D3 and D0 respectively lead to the lowest and highest numbers of collapse. D3 results seem very close to those with D1 configuration, and previous FPI and $EI(UC)$ indices are useful to understand the highest risk of propagation and the lowest energy demand that distinguish D3 and D1 settings. Otherwise, if D2 and D4 are close according to FPI and $EI(UC)$ values (Figure 12), collapse repartition category helps us have a clearer distinction, in particular for C3 and C4 scenarios. This first level of analysis leads to D0, D2, D4, D1 and D3 classification from the less to the more robust structure.

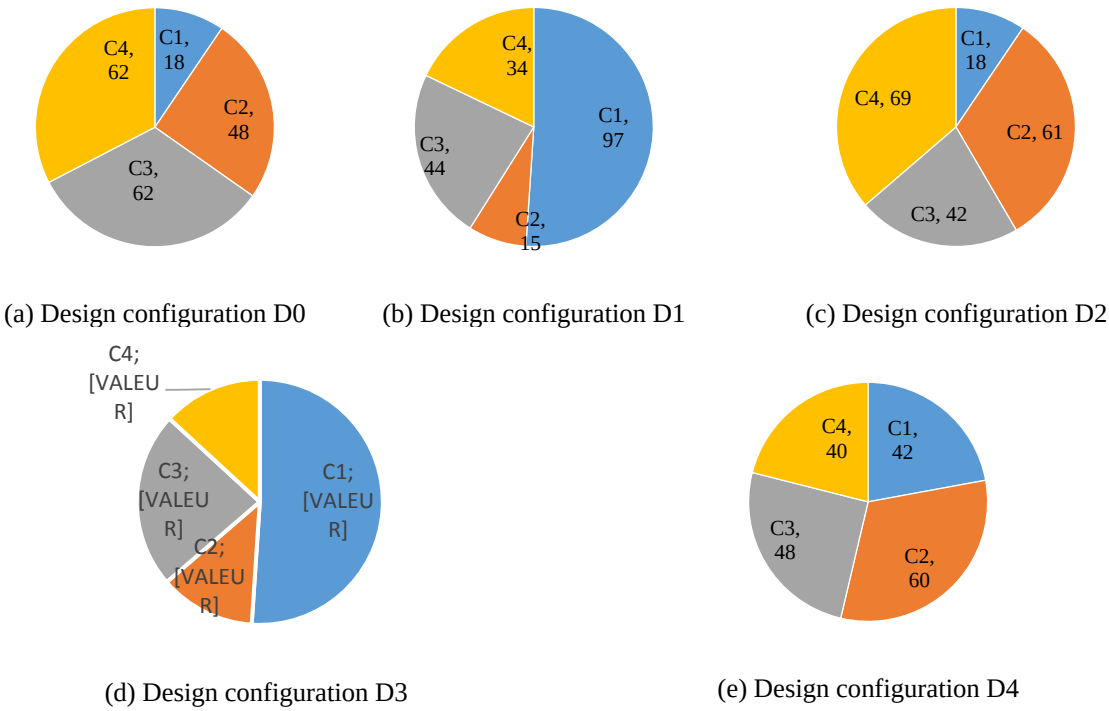

(a) Design configuration D0 (b) Design configuration D1 (c) Design configuration D2

(d) Design configuration D3 (e) Design configuration D4

Figure 13. Number of local failure scenarios within categories C1 to C4 for design configurations D0, D1, D2, D3 and D4.

5.3. Analysis at the Pareto front level

To further discriminate the scenarios that minimize initial failure demand and maximize propagation response, the robustness analysis is now presented for each configuration at the Pareto front level according to the Pareto fronts S1, S2 and S3 computations. Figure 14 illustrates S1 Pareto fronts for D0 to D4 configurations, where each dot corresponds to one or several scenario(s). Figure 15 shows the number of total scenarios constitutive of Pareto fronts S1, S2 and S3 for each configuration. Some scenarios being present in several Pareto fronts, the total number of unique scenarios (*US*) is lower than the sum of the different front scenarios.

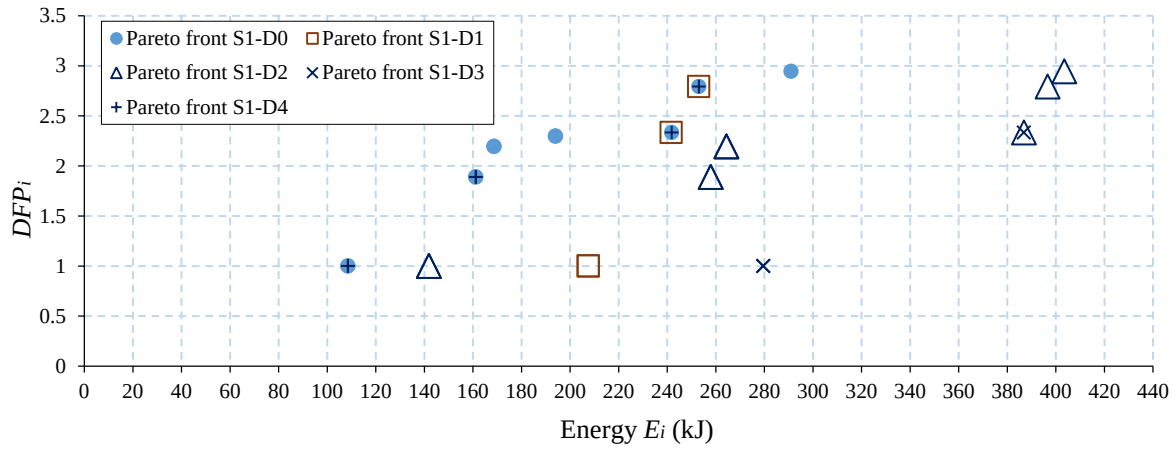

Figure 14. Identification of non-dominated solutions for the design configurations D0, D1, D2, D3 and D4 when simultaneously minimizing E_i and maximizing DFP_i (Equation 6).

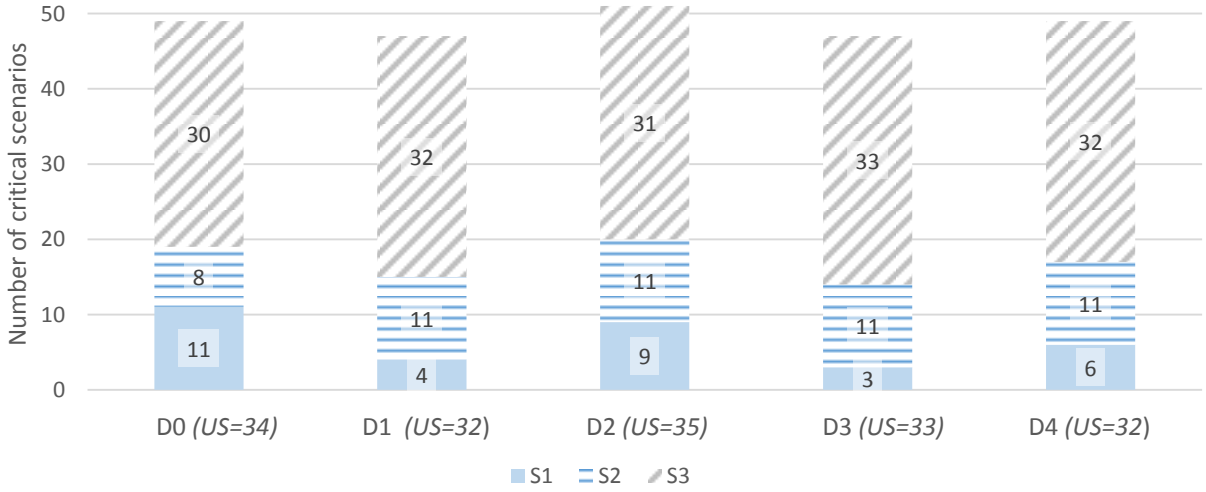

Figure 15. Number of scenarios in Pareto fronts S1, S2 and S3 for configuration D0 to D4 – *US* is the number of unique scenarios.

The unacceptable scenarios are determined as the matching scenarios between Pareto fronts S1, S2, S3 and the threshold on $\mathcal{M}(CP_i)$ (90 m herein) as illustrated in Figure 16 and listed in Table 14. As an example for D3 configuration, seven critical situations are identified amongst the 47 Pareto front scenarios in Figure 15, knowing that there are 29 scenarios with $\mathcal{M}(CP_i) \geq 90$ m (Figure 16).

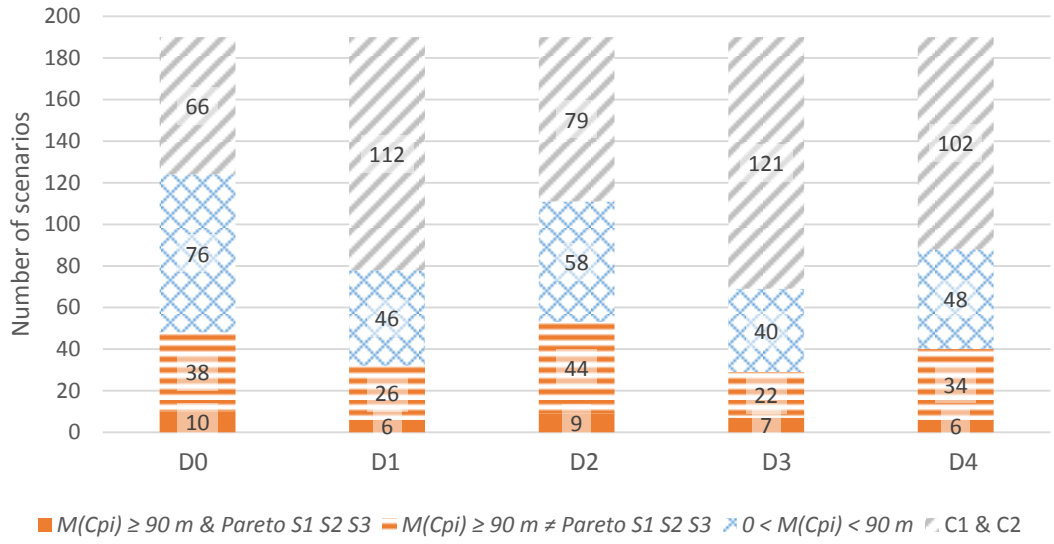

Figure 16. Analysis of disproportionate collapse at the Pareto front level for D0 to D4 configurations.

D0	**76**	77	78	**81**	82	83	126	127	**128**	129
D1	123	**126**	**127**	133	168	173				
D2	**73**	76	77	**81**	82	88	126	127	**128**	
D3	122	**126**	132	163	168	173	178			
D4	72	**76**	**81**	87	126	**127**				

Table 14. Identification of unacceptable scenarios ($\mathcal{M}(CP_i) \geq 90$ m) belonging to S1, S2 or S3, the scenarios in bold being those already identified using FPI and $EI(UC)$.

The final step of this Pareto front level approach is to compare the performance between the five different configurations by discriminating non-dominated solutions of the Pareto fronts determined previously, also considering design configurations. The bi-objective problems of Equation 6, 7 and 8 are respectively solved on the three sets of non-dominated scenarios for each design configuration merging: (i) S1-D0 to S1-D4, (ii) S2-D0 to S2-D4 and (iii) S3-D0 to S3-D4, respectively. As an example, Figure 17 shows the Pareto front for the S1 optimization problem (to be compared to Figure 14). The new Pareto front is named Pf-S1, fronts 2, 3 and 4 being some lower fronts.

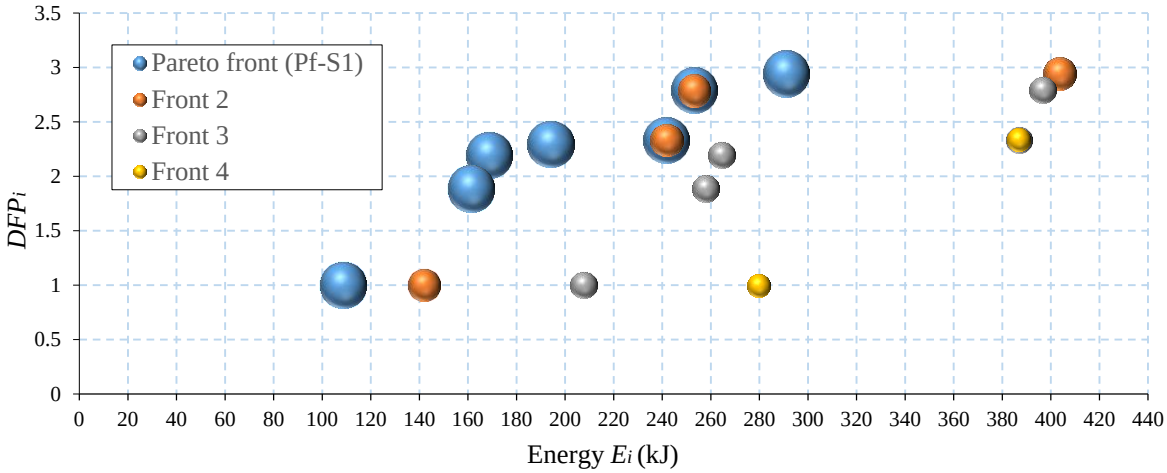

Figure 17. Identification of non-dominated scenarios of the Pareto fronts S1-D0, S1-D1, S1-D2, S1-D3 and S1-D4 according to Equation 6.

For each configuration D0 to D4, this additional bi-objective problem allows identifying the scenarios of the individual Pareto front (S1-D0 to S1-D4) that are constitutive of the corresponding global Pareto front (Pf-S1). Figure 18 presents for S1, S2, S3 and each configuration D0 to D4 the number of these scenarios (where global Pareto fronts are noted Pf-S2 and Pf-S3 for S2 and S3 optimization problems, respectively). As an example, the five configurations can be sorted regarding the total number of Pareto front scenarios where D0, D2, D4, D1 and D3 are the lowest to the more robust settings. The ranking is the same as in Section 5.2, with an advanced analysis of critical non-dominated scenarios.

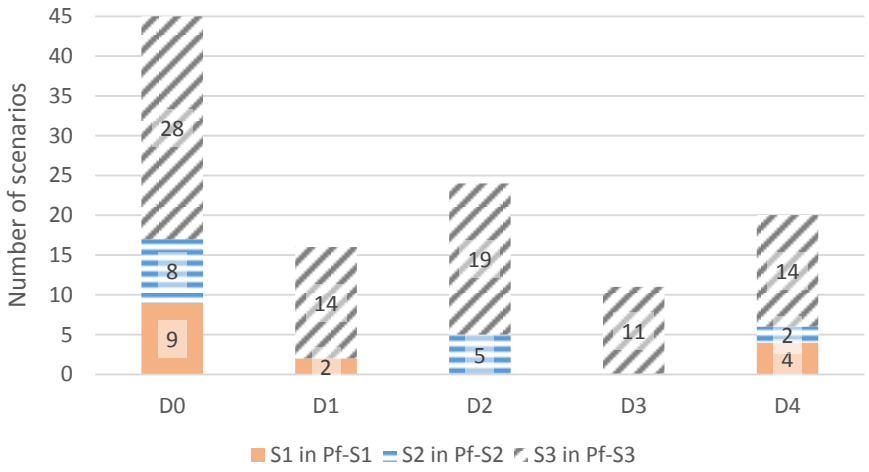

Figure 18. Number of scenarios regarding S1 in Pf-S1, S2 in Pf-S2 and S3 in Pf-S3 for D0 to D4 configurations.

The choice between the three bi-objective problems corresponds to some different understanding of the robustness concept, but always with the same approach of identifying initial failure scenarios with minimal causes and maximal consequences. Some feedback on the five structural variations (D0 to D4) shows that the scenarios found with the second bi-objective problem are systematically obtained with the first and third bi-objective problem. The complementary between the first and the third Pareto front seems sufficient. However further analysis considering different structural typology should be conducted to confirm these results.

6. Conclusions

The main purpose of this work is to develop a strategy to assess the robustness of a structure with respect to the requirements in design codes such as Eurocodes (NF EN 1991-1-7 2007) where a local structural failure should not lead to a disproportionate damage propagation.

To provide a general assessment of structural robustness by studying a large number of scenarios in a reasonable computation time, the structural modelling strategy proposed by El Hajj Diab et al. (2021) was used herein. This strategy, based on an iterative coupling between the yield design approach and a non-linear finite element analysis allows us to investigate the propagation occurrence and magnitude in a structure. A major benefit of this coupling modelling is to integrate the possible redistribution of efforts in the non-linear range and to develop an alternative equilibrium state, while computational time remains significantly lower than with a full finite element modelling analysis.

A bi-indicator approach is adopted to describe the sensitivity of a structure to different scenarios of initial failure. First, the Failure Propagation Index (FPI) is proposed with the aim

to quantify the largest propagation extent among all scenarios of local failure occurrence. This index is computed using the $\mathcal{M}(IDP_i)$ and the $\mathcal{M}(CP_i)$ metrics defined as the Initial Damage Part and the Final collapse parts of each scenario i. Second, the Energy Index ($EI(UC)$), identifies the lowest energy need for local failure scenarios that lead to an unacceptable collapse. On the one hand, the energy need is computed according to a specific or an arbitrary load profile that can be sufficient to compare scenarios performances. On the other hand, the unacceptable collapse threshold is defined accordingly to a user threshold (UC) of failure extent. If no threshold is defined, UC can be assumed as the first $\mathcal{M}(CP_i)$ value that is greater than $\mathcal{M}(IDP_i)$, which means an initiation of progressive collapse. These two criteria, FPI and $EI(UC)$, based on propagation extent or energy related to initial failure scenario have been considered separately, and also simultaneously, since robustness can be understood as a combined research of minimal causes with maximal consequences. A methodology relying on the concepts of three distinct bi-objective optimization is also proposed to specifically identify the scenarios with minimal initial magnitude (based on energy or part of the structure initially affected) and maximal extent (based on failure propagation ratio, or total part of the structure that failed). This set of bi-objectives critical scenarios corresponds to three complementary Pareto fronts. Hence, the unacceptable scenarios are those that simultaneously fit the three sets of Pareto fronts scenario, also reaching a threshold of maximal damage extent (UC).

The proposed methodology is applied to steel frame-building case study where 190 failure scenarios are tested. Combining the coupling modelling strategy and the proposed robustness assessment method quickly leads to a robustness quantification of the structure and an identification of its most critical scenarios.

This approach is then used to compare the performance of the initial structure with four others configurations including retrofitting aspects. The FPI and the $EI(UC)$ directly lead to find the strongest and the weakest configurations, while the three bi-objectives problems enable to

identify the critical scenarios of each configuration and their occurrence, then allowing to fully classify the different configurations. The proposed case study illustrates the usefulness and versatile aspects of the proposed methodology as (i) the structural modelling can be done with the coupling approach or any other dealing with progressive collapse, and (ii) each robustness indicator can be used separately or together.

To provide a wide overview of the several types of scenarios (C1, C2, C3 or C4), the proposed concepts are illustrated with a low-rise framed building that commonly offers larger redistribution possibilities comparatively to a high-rise structure. However, even, if less redundancy is expected, the proposed strategy could also be used on tall framed buildings. More generally, the method could be used in further applications with different structural systems, provided that an initial and a final damage extent of the system can be measured.

This work aims to be used in the future, either by providing some recommendations on design for robustness based on prior calculation using the proposed approach or by integrating calculations within a risk-based analysis, as recently considered in other studies focusing on damage propagation (Droogné et al. 2018, Praxedes et al. 2021, Praxedes & Yuan 2021, 2022), in link with the evolution of standards related to the development of technical recommendations for robustness characterization.

REFERENCES

Agarwal, J., England, J., 2008. Recent developments in robustness and relation with risk. *Proceedings of the Institution of Civil Engineers - Structures and Buildings 161*, 183–188. https://doi.org/10.1680/stbu.2008.161.4.183.

Alashker, Y., El-Tawil S. and Sadek, F. (2010). Progressive collapse resistance of steel-concrete composite floors. *Journal of Structural Engineering*, 136(10). DOI:10.1061/(ASCE)ST.1943-541X.0000230.

Arup, 2011. Review of international research on structural robustness and disproportionate collapse. Department for Communities and Local Government, and Centre for the Protection of National Infrastructure, London.

ASCE, A.S. of C.E., 2016. Minimum design loads and associated criteria for buildings and other structures (ASCE/SEI 7-16).

Biondini, F., Frangopol, D.M., Restelli, S., 2008. On Structural Robustness, Redundancy, and Static Indeterminacy, in: Structures Congress 2008. Presented at the Structures Congress 2008, American Society of Civil Engineers, Vancouver, British Columbia, Canada, pp. 1–10. https://doi.org/10.1061/41016(314)237.

Bleyer, J., de Buhan, P., 2013. Yield surface approximation for lower and upper bound yield design of 3d composite frame structures. *Computers & Structures*, 129, 86-98.

Bontempi, F., Giuliani, L.G., Gkoumas, K., 2007. Handling the exceptions: Robustness assessment of a complex structural system. *Proceedings of the 3rd international conference on structural engineering, mechanics and computation (SEMC 2007)*, 1747-1752.

Botte, W., Caspeele, R., Gouverneur, D., Taerwe, L., 2014. Influence of membrane action on robustness indicators and a global resistance factor design, in: Bridge Maintenance, Safety, Management and Life Extension. CRC Press, pp. 2038–2046.

Brett, C., Lu, Y., 2013. Assessment of robustness of structures: Current state of research. *Frontiers of Structural and Civil Engineering* 7, 356–368. https://doi.org/10.1007/s11709-013-0220-z.

Brozzetti, J., 1996. Eurocode 3 calcul des structures en acier. Partie 1-1, Règles générales et règles pour les bâtiments.

DCLG, 2013. The building regulations 2010 - structure: approved document A.

Deb, K., Pratap, A., Agarwal, S., Meyarivan, T., 2002. A fast and elitist multiobjective genetic algorithm: NSGA-II. *IEEE Transactions on Evolutionary Computation* 6, 182–197. https://doi.org/10.1109/4235.996017.

COST Action TU0601, 2011. Robustness of Structures - theoretical framework on structural robustness.

De Biagi, V.D., Kiakojouri, F., Chiaia, B. and Sheidaii, M.R. (2020). A Simplified Method for Assessing the Response of RC Frame Structures to Sudden Column Removal. *Appl. Sci.* 2020, *10*, 3081. https://doi.org/10.3390/app10093081.

De Biagi V. Energy redistribution patterns in damaged elastic frames, *Int J Mech Sciences* 194:1062016.

Demonceau, J.-F., 2008. Steel and composite building frames: sway response under conventional loading and development of membrane effects in beams further to an exceptional action. Université de Liège.

Department of Defense (DoD).2005. UFC 4-023-03: Design of buildings to resist progressive collapse. Washington, DC (US).

Department of Defense (DoD). 2009. UFC 4-023-03: Design of buildings to resist progressive collapse. Washington, DC (US).

Department of Defense (DoD). 2016. Review of UFC 4-023-03: Design of buildings to resist progressive collapse. Washington, DC (US).

Droogné, D., Botte, W., Caspeele, R., 2018. A multilevel calculation scheme for risk-based robustness quantification of reinforced concrete frames. *Engineering Structures* 160, 56–70. https://doi.org/10.1016/j.engstruct.2017.12.052.

El Hajj Diab, M., 2019. Analyse de la robustesse structurale, caractérisation des actions accidentelles et/ou exceptionnelles et de leurs effets sur les structures. Thèse de l'Université Paris-Est.

El Hajj Diab, M., Orcesi, A., Desprez, C., Bleyer, J., 2021. A progressive collapse modelling strategy coupling the yield design theory with nonlinear analysis. *Engineering Structures* 241, 111832.

Faber, M.H., Maes, M.A., Straub, D., Baker, J., 2006. On the Quantification of Robustness of Structures, in: Volume 3: Safety and Reliability; Materials Technology; Douglas Faulkner Symposium on Reliability and Ultimate Strength of Marine Structures.

Faber, M.H., 2007. Risk and Safety in Civil Engineering, *Lecture notes*, ETH, Zurich.

fib, 2012. Model Code 2010 - Final draft, Volume 2.

Filippou, F.C., Constantinides, M., 2004. FEDEASLab getting started guide and simulation examples. *Technical report* NEESgrid-TR22.

Foley, C.M. et al (2007) Robustness in Structural Steel Framing Systems, American Institute of Steel Construction, Inc.

Fu F., 2009 Progressive collapse analysis of high-rise building with 3-D finite element modeling method. *J Constr Steel Res* 65:1269-78.

Gerasimidis, S. (2014), Analytical assessment of steel frames progressive collapse vulnerability to corner column loss, *Journal of Constructional Steel Research*, 95. https://doi.org/10.1016/j.jcsr.2013.11.012.

Gerasimidis, S. and Sideri, J. (2016), A new partial-distributed damage method for progressive collapse analysis of steel frames, Journal of Constructional Steel Research, 119, 233-245.

Ghosn, M., Dueñas-Osorio, L., Frangopol, D.M., McAllister, T.P., Bocchini, P., Manuel, L., Ellingwood, B.R., Arangio, S., Bontempi, F., Shah, M., Akiyama, M., Biondini, F., Hernandez, S., Tsiatas, G., 2016. Performance Indicators for Structural Systems and Infrastructure Networks. *Journal of Structural Engineering*, 142, F4016003, https://doi.org/10.1061/(ASCE)ST.1943-541X.0001542.

GSA, 2003. Progressive Collapse Analysis and Design Guidelines for New Federal Office Buildings and Major Modernization Projects.

GSA, 2013. Alternative path analysis and design guidelines for progressive collapse resistance.

Haberland, M., 2007. Progressive collapse and robustness. Structural Analysis and Steel structures Institute.

Huvelle, C., Hoang, V.-L., Jaspart, J.-P., Demonceau, J.-F., 2015. Complete analytical procedure to assess the response of a frame submitted to a column loss. *Engineering Structures* 86, 33–42. https://doi.org/10.1016/j.engstruct.2014.12.018.

Huvelle, C., 2011. Contribution à l'étude de la robustesse des structures de bâtiments - Prise en compte de la plastification progressive de la partie de la structure "non directement affectée" par l'événement exceptionnel considéré. Université de Liège - Faculté des Sciences Appliquées.

Izzuddin, B.A., Vlassis, A.G., Elghazouli, A.Y., Nethercot OBE, D.A., 2007. Assessment of progressive collapse in multi-storey buildings. *Proceedings of the Institution of Civil Engineers - Structures and Buildings* 160, 197–205.

Izzuddin, B.A., Vlassis, A.G., Elghazouli, A.Y., Nethercot, D.A., 2008. Progressive collapse of multi-storey buildings due to sudden column loss — Part I: Simplified assessment framework. *Engineering Structures* 30, 1308–1318. https://doi.org/10.1016/j.engstruct.2007.07.011.

Jaspart, J.P., Demonceau, J.F., Ludivine, C., 2011. Robustness of steel and composite building structures. Presented at the 7th National conference on steel structures, Greece, Volos.

JCSS, 2008. Risk assessment in engineering – principles, system representation and risk criteria.

Kagho-Gouadjio, N.C., Orcesi, A.D. Cremona, C. & Marcotte, C. (2015). Quantification of structural robustness: application to the study of a prestressed concrete beam, Mechanics & Industry, 16(1), 104.

Khandelwal, K., El-Tawil, S., 2011. Pushdown resistance as a measure of robustness in progressive collapse analysis. Eng. Struct. 33, 2653–2661. https://doi.org/10.1016/j.engstruct.2011.05.013

Kiakojouri, F., De Biagi, V., Sheidaii, M.R., Chiaia, B. (2020). Progressive collapse of framed building structures: current knowledge and future prospects, *Engineering Structures* 206:110061 10.1016/j.engstruct.2019.110061.

Le, T.N., 2013. Nonlinear dynamics of lexible structures using corotational beam elements. INSA Rennes.

Le, T.-N., Battini, J.-M., Hjiaj, M., 2014. Corotational formulation for nonlinear dynamics of beams with arbitrary thin-walled open cross-sections. *Computers & Structures* 134, 112–127. https://doi.org/10.1016/j.compstruc.2013.11.005.

Le, T.-N., Battini, J.-M., Hjiaj, M., 2011. Efficient formulation for dynamics of corotational 2D beams. *Computational Mechanics* 48, 153–161. https://doi.org/10.1007/s00466-011-0585-6.

Marchand, K.A., Alfawakhiri, F., 2005. Facts for Steel Buildings-Blast and Progressive Collapse.

NF EN 1990, 2003. Basis of structural design. Comité européen de Normalisation (CEN).

NF EN 1991-1-1, 2003. Eurocode 1, Actions on structures, Part 1-1: General actions — Densities, self weight, imposed loads for buildings.

NF EN 1991-1-7, 2007. Eurocode 1 - Actions on structures - Part 1-7: General actions - Accidental actions. European Committee for Standardization (CEN).

Pantidis P. and Gerasimidis, S. (2018). Progressive collapse of 3D steel composite buildings under interior gravity column loss, *Journal of Constructional Steel Research*, 150, 60-75.

Praxedes C, Yuan XX, He XHC. 2021. A risk-based robustness index for progressive collapse analysis of structures. *Structure and Infrastructure Engineering*. DOI: 10.1080/15732479.2020.1851730

Praxedes C, Yuan XX. 2021. Robustness assessment of reinforced concrete frames under progressive collapse hazards: a novel risk-based framework. *Journal of Structural Engineering*, ASCE. 147(8): 04021119. DOI: 10.1061/(ASCE)ST.1943-541X.0003075

Praxedes C, Yuan XX. 2022. Robustness-oriented optimal design for reinforced concrete frames considering the large uncertainty of progressive collapse threats. *Structural Safety*. 94: 102139. https://doi.org/10.1016/j.strusafe.2021.102139.

Sideri J., Mullen, C., Gerasimidis, S. and Deodatis, G. (2017). Distributed Column damage effect on progressive collapse vulnerability in steel buildings exposed to an external blast event, ASCE *Journal of Performance of Constructed Facilities*, 31(5): 04017077.

Spacone, E., Filippou, F.C., Taucer, F.F, 1996. Fibre beam-column model for non-linear analysis of R/C frames: part I. Formulation. *Earthquake Engineering & Structural Dynamics* 25, 711–725.

Starossek, U., Haberland, M., 2010. Disproportionate Collapse: Terminology and Procedures. *Journal of Performance of Constructed Facilities* 24, 519–528. https://doi.org/10.1061/(ASCE)CF.1943-5509.0000138.

Starossek, U., Haberland, M., 2011. Approaches to measures of structural robustness. *Structure and Infrastructure Engineering* 7, 625–631. https://doi.org/10.1080/15732479.2010.501562.

Ventura, A., De Biagi, V. and Chiaia, B. (2018). Structural robustness of RC frame buildings under threat-independent damage scenarios. *Structural Engineering and Mechanics*. 65. 689-698. 10.12989/sem.2018.65.6.689.

Vrouwenvelder, T., 2008. Treatment of risk and reliability in the Eurocodes. *Proceedings of the Institution of Civil Engineers - Structures and Buildings* 161, 209–214. https://doi.org/10.1680/stbu.2008.161.4.209.